Measurements of Dynamic Surface Changes by Digital Holography for *In Situ* Plasma Erosion Applications

C. D. Smith,[1,a)] T. M. Biewer,[2] T. E. Gebhart,[2] E. G. Lindquist,[3] and C. E. Thomas[4]

[1]*Mechanical, Aerospace, & Biomedical Engineering Department, University of Tennessee, Knoxville, Tennessee 37996, USA*
[2]*Fusion Energy Division, Oak Ridge National Laboratory, Oak Ridge, Tennessee 37831, USA*
[3]*Nuclear Engineering Department, University of Tennessee, Knoxville, Tennessee 37996, USA*
[4]*Third Dimension Technologies, Oak Ridge, Tennessee 37830, USA*

(Presented XXXXX; received XXXXX; accepted XXXXX; published online XXXXX)
There are currently few viable diagnostic techniques for *in situ* measurement of plasma facing component erosion. Digital holography is intended to fill this gap. Progress on the development of single and dual CO_2 laser digital holography diagnostics for *in situ* plasma facing component erosion is discussed. The dual laser mode's synthetic wavelength allows the measurable range to be expanded by a factor of ~400 compared to single laser digital holography. This allows the diagnostic to measure surface height changes of up to 4.5 µm in single laser mode and up to 2 mm in dual laser mode. Results include *ex situ* measurements of plasma eroded targets and also dynamic measurements of nm and µm scale motion of a target mounted on a precision translation stage. Dynamic measurements have successfully been made with the system operating in both single and dual laser modes, from ~50 nm to ~4 µm in single laser mode, and up to ~400 µm in dual laser mode (limited only by the stage speed and camera acquisition duration). These results demonstrate the feasibility of using digital holography to characterize plasma facing component erosion dynamically, i.e. during plasma exposure. Results of proof-of-principle *in situ* digital holographic measurements of targets exposed to an electrothermal arc plasma source are presented.

I. INTRODUCTION

Plasma facing components (PFCs) in fusion devices are subject to surface-deforming plasma effects, especially during highly transient events. These effects may include erosion of the surface, redeposition of eroded material, and implantation into the surface. Plasma-material interaction (PMI) is therefore an important area of research interest for large scale fusion projects such as ITER.[1] While various plasma diagnostics and *ex situ* material measurement techniques have been applied to PMI studies,[2] there is not currently a method to monitor 3-D surface deformation *in situ*; Digital Holography (DH) has been proposed as a solution to this problem.[3,4] A DH system has been established and characterized at the Oak Ridge National Laboratory (ORNL) for measurements of plasma-exposed surfaces.[4-8] The system includes a unique capability of producing dual-laser holograms which allows the system to measure surface features on the nm to mm levels. Measurements have been successfully performed on targets with artificial surface height gradients as well as plasma-exposed targets. The developmental goal was ultimately to couple the DH system with an electrothermal (ET) arc source to carry out a proof-of-principle demonstration of *in situ* measurement of a plasma-exposed surface. In this work, DH characterization efforts toward this end are reported, including *ex situ* measurement of erosion on targets exposed to the ET-arc and temporally resolved surface displacement measurements of a moving mirror target in simulation of whole-surface average height changes occurring during an erosion event, which informed the *in situ* measurement demonstration. Results of the successful demonstration are described, including holograms taken before, during, and after the plasma event.

[a)]Author to whom correspondence should be addressed: csmit121@tennessee.edu.

II. TECHNIQUE

Digital holography (DH) produces topographical information from a holographic image of a target surface. A reference laser beam interferes with an object laser beam reflected from the target to produce fringe patterns which form the holographic image. Phase information ϕ is then extracted from the spatial Fourier transform of the hologram as a function of wavelength λ and path length l given by Equation 1.

$$\phi = \frac{2\pi l}{\lambda} \quad (1)$$

Taking the path length as a function of the phase information thus provides the z-axis surface height at every point in the x-y image plane.

The phase information is bounded by 0 and 2π, which limits the maximum measurable surface height; since the image is reflected, the recorded hologram doubles the measurement of a surface feature's actual height and therefore the effective upper measurable height limit of an object is equal to half of the laser wavelength in single laser DH. Surface features that exceed this limit appear as "jumps" and are difficult to interpret. The ORNL DH system's upper limit in single laser mode is ~4.5 µm. Dual laser DH allows the maximum measurable surface height to be greatly increased via formation of a "synthetic" wavelength. This factor arises by tuning laser 2 to a slightly larger wavelength than laser 1. Division of a laser 1 hologram by a laser 2 hologram (similar to flatfield correction for single laser holograms) produces differential phase information given by the following:

$$\phi_1 - \phi_2 = 2\pi l\left(\frac{\lambda_2-\lambda_1}{\lambda_1\lambda_2}\right) = \frac{2\pi l}{\lambda_{synth}} \quad (2)$$

In this equation, the synthetic wavelength λ_{synth} is much larger than either of the single lasers' wavelengths alone and therefore enlarges the equivalent maximum path length afforded by the phase range. The ORNL DH system's lasers are tuned to wavelengths of 9.25 µm and 9.27 µm, and therefore it has a λ_{synth} wavelength multiplier of ~440, which raises the upper limit of surface height measurement to ~2 mm in dual laser mode. Detailed description of the technique has been given in other publications.[4] Flatfield correction may also be performed on differential holograms as shown by Equation 3:

$$\Delta\phi_1 - \Delta\phi_2 = \left(\phi_i - \phi_j\right)_1 - \left(\phi_i - \phi_j\right)_2 = \frac{2\pi(l_i - l_j)}{\lambda_{synth}} \quad (3)$$

A hologram with wavelength λ_1 and phase data ϕ_i is flatfield corrected with another hologram of the same wavelength but different phase data ϕ_j, which produces $\Delta\phi_1$ as a function of path length difference. The same correction is performed for holograms with wavelength λ_2, and then dual wavelength holographic subtraction is performed on the two quantities. Flatfield correction allows analysis of recorded hologram sequences capturing temporal surface changes by subtracting a reference frame from all other frames in a sequence. The corrected frames then exhibit the temporal evolution of surface difference from the reference frame.

III. EXPERIMENTAL SETUP

A. Digital Holography and Electrothermal Arc Source

The ORNL DH system has been described in detail previously.[4,5] A schematic is shown in Figure 1. In brief, it utilizes two CO_2 lasers with acousto-optic modulators (AOMs) acting as secondary shutters aligned to the same reference and object beam paths so that the same target region of interest (ROI) can be imaged using either or both of the lasers depending on whether single or dual laser mode is used. The beams image a target circular area ~8 mm in diameter at magnification M = 1 with 10 inch (25.4 cm) focal length ZnSe lenses. The detector is a FLIR SC4000 infrared (IR) camera with a typical window size setting of 256 x 256 pixels for 500 Hz imaging. In single laser mode, holographic frames utilizing one laser are therefore captured at a time increment of 2 ms. In dual laser mode the AOMs alternately open and close such that the holographic frames switch between Laser 1 and 2 at this 2 ms time increment. The laser exposure time on the IR camera is typically 13 µs and can be raised for targets with low reflectivity. The standard configuration for *ex situ* imaging allows the target object to be mounted on the same optical table as the DH system, while for *in situ* imaging the target is located off the table.

The ORNL ET-arc system simulates transient fusion plasma events.[9] It produces directed plasma to impact a target surface inside a vacuum vessel using helium at 10 Torr pressure as the fill gas. The plasma has ~1.2 kJ source energy and transmits ~1 GW/m^2 heat flux over ~2 ms, with an angle of incidence of 45° under its configuration for *ex situ* DH characterization.

B. Translation Stage

DH motion detection characterization was performed to demonstrate the system's capability of capturing frame-by-frame changes in surface height in simulation of an erosion event. A flat mirror was mounted on a New Focus linear translation stage (Model No. 9063-B with model 8310 actuator) to provide a moving target capable of performing translations on the order of tens of nm. The target was translated along the laser axis so that forward motion of the target mirror was detected by the DH system as an increase in surface height and backward motion as a decrease. The actuator was operated in closed-loop mode in which it has an optical encoder resolution of 63.5 nm. Its bi-directional and uni-directional repeatability are ±1 µm and ±100 nm respectively.

C. Configuration for In Situ Measurements

The DH system was coupled with the ET-arc as shown in Figure 1. Modifications were made to the DH system for this implementation.[10] The modified system replaces the original lenses with new 15 inch (38.1 cm) focal length lenses, which moves the focal position off the optical table to accommodate the target location inside the ET-arc chamber and produces a magnification of M = 3 at the detector. The holographic spatial resolution was consequently lowered and the field-of-view on the target was increased by the lens change. The ET-arc was also modified[11] to change the plasma angle of incidence on the target to 35°, and its operational parameters for the *in situ* demonstration were changed from those of the *ex situ* characterization to a plasma source energy of ~2 kJ and pulse duration of ~1 ms.

IV. RESULTS AND DISCUSSION

A. *Ex Situ* Erosion Measurement

Ex situ DH imaging experiments of 304 stainless steel surfaces exposed to ET-arc plasma were carried out to characterize the DH system's potential applicability for *in situ* coupling with the ET-arc. The full results of the characterization can be found in another work,[12] and a brief summary of the experiment is provided here. Stainless steel "step" targets were manufactured with a typical roughness average of ~600-800 nm and including a removable cover plate ~1.5 mm thick. They were aligned in the ET-arc chamber such that some of the incoming plasma would strike the target at the edge of the cover plate; this design was intended to produce a relatively undamaged "shadowed" region adjacent to the plasma strike zone on the base plate which would act as a fiducial for DH measurements. The cover plate was removed during DH imaging to further allow surface height normalization by comparison of the untouched covered region for each level of plasma exposure. Soot deposits were not cleaned from the targets after plasma exposure to allow the *ex situ* DH characterization to simulate *in situ* imaging as much as possible. Two step–targets were imaged with the DH system pre- and post-plasma exposure with up to 9 total exposures repeated on the same target. The key finding from this study was that average measured plasma erosion on the step targets was 151 nm per shot,[12] which should be measurable *in situ* based on the performance characteristics of the DH system and ET-arc (including vibrational noise effects and thermal growth of the plasma-exposed target).[8] Actual (successful) *in situ* measurements are shown later in this paper.

B. Single Laser Holographic Motion Detection

Dynamic motion detection experiments were conducted for single and dual laser modes respectively.[10] Translation events for displacements up to 1 µm were holographically recorded at 50 Hz and 500 Hz. The resulting holographic "movies" displayed the z-axis phase change of the x-y planar surface resulting from the change in object beam path length caused by the translation of the target mirror. Ergo, a holographic surface with a starting position (i.e. mean z-axis value for the x-y surface) defined at 0 would exhibit a clearly discernible phase displacement over time corresponding to the movement of the target mirror forward or backward along the laser axis. A total of 500 sequential holographic frames were recorded for each movie, resulting in 10 s of recorded mirror motion per 50 Hz movie, and 1 s of recorded motion for the 500 Hz movies. The holographic frames of each movie were processed by flatfield correction with the first frame of the set, so that the processed phase images showed the relative surface change of each frame compared to the initial position.

Analysis of the surface change was performed by plotting the mean phase value ± standard deviation for each frame. The translations therefore appeared in step form on

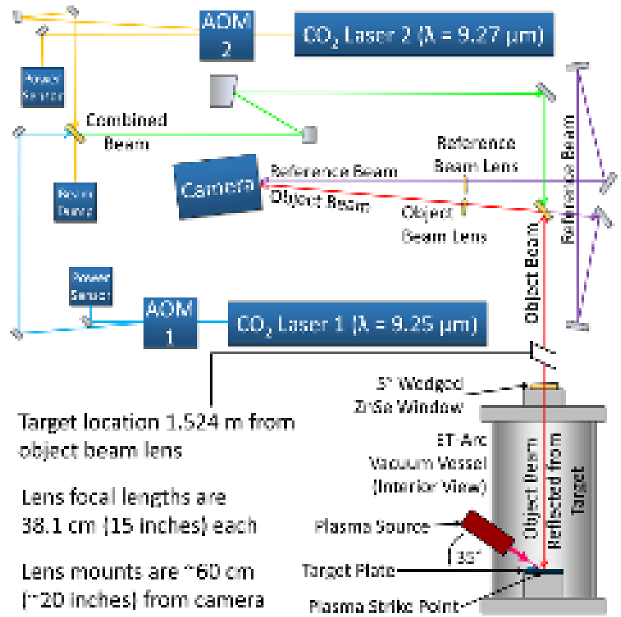

FIG. 1. (Color online). Schematic of the DH system coupled with the ET-arc source for *in situ* holography.

the plots. When possible, multiple translation events showing movement from and return to the initial position were recorded (the 10 s window for 50 Hz recordings easily enabled this but only single movement/return events could be recorded within the 1 s window at 500 Hz). The first movement/return displacements were tabulated for each programmed translation (see Table I). Note that in some cases two displacements were not able to be captured either due to recording time limitation or holographic phase noise. Plotting the displacements with their corresponding programmed translation values (Figure 2) reveals an expected linearity and demonstrated the viability of this method of motion analysis. Generally, the displacements showed high repeatability in that the movement and return motions per recording were close in value to each other. Note that the programmed displacement shown, representing the linear increase in surface displacement as the number of translation counts increases, is calculated from a motion increment of 51 nm/count; this value is below the actuator's minimum incremental motion (i.e. optical encoder resolution), however repeated DH measurements

TABLE I. Single Laser DH Detected Motion.

Translation (Counts)	50 Hz Detected Surface Height (nm), Displacement and Return	500 Hz Detected Surface Height (nm), Displacement and Return	Programmed Translated Height (nm), 51 nm Per Count
1	Undiscernible	76, 67	51
3	128, 117	114, 115	153
5	159, 158	175, 176	256
10	301, 389	384, 390	511
15	595, 632	687, N/A	767
18	998, 885	972, N/A	920

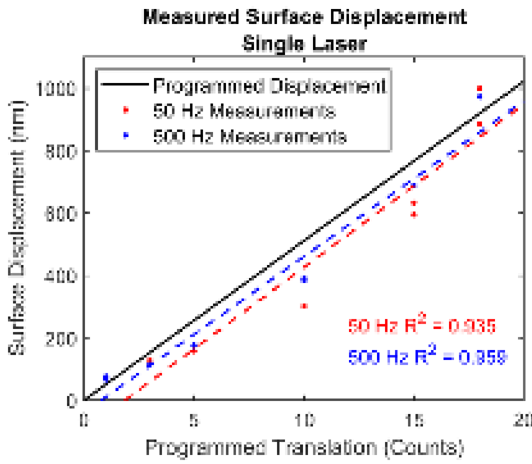

FIG. 2. (Color online). Single laser DH detected motion vs. programmed translation.

with the same number of counts showed variations corresponding to measured incremental motions ranging from ~43 to ~63 nm. The actuator's bi-directional repeatability of ±1 µm as well as measurement error from phase image noise (to be described in detail in the following paragraphs) may account for the apparent discrepancy.

Phase noise interfered with the results of this analysis; noise levels of ~100 nm for 50 Hz holography affecting the

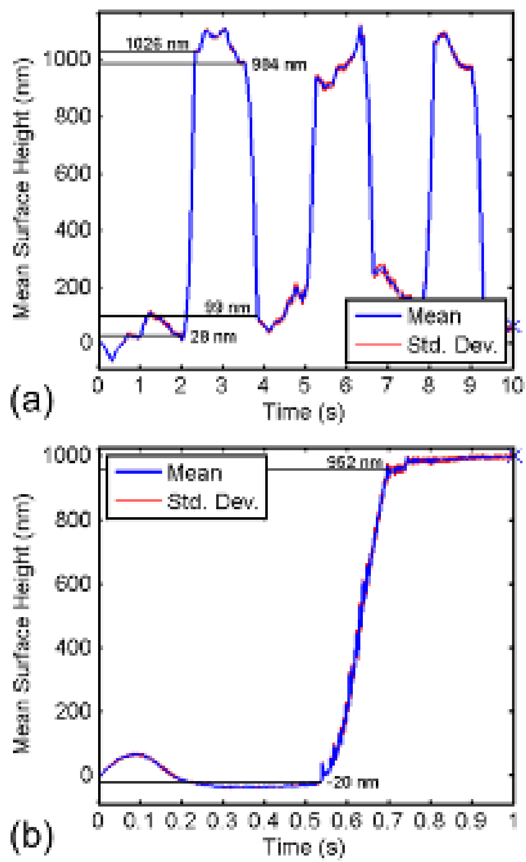

FIG. 3. (Color online). (a) ~1 µm detected motion from a 50 Hz recording. (b) ~1 µm detected motion from a 500 Hz recording. Both results show 18 count movements, with higher measured surface height fidelity frame-to-frame in the 500 Hz recording vs. capability of capturing multiple events in the longer 50 Hz recording.

phase values of a single holographic image as well as the phase difference between temporally displaced frames from an initial image are known characteristics of the DH system.[8] Noise effects worsen over time due to the increase in prominence of low frequency vibration, accumulation of systematic noise throughout recordings, and increase in camera temperature after shutoff of its cryo-cooler. Additionally, frame-to-frame noise is on the order of tens of nm for 50 Hz holography. A 10 s movie recorded at 50 Hz therefore accumulates noise more and more severely over its duration. If a 1 s recording is performed at 500 Hz, then noise is significantly reduced at the cost of available recording time. At that rate, typical frame-to-frame noise is only a few nm, and the short recording time does not allow low frequency noise and systematic effects to build up. The motion analysis therefore exhibited the effects of noise in the improved linearity of the displacements detected at 500 Hz versus those detected at 50 Hz. This can be interpreted as the 500 Hz movies' higher fidelity of the mean holographic surface phase value to the actual target's translated displacement since noise is lower. Conversely, the 50 Hz recordings were more prone to producing mean surface phase values with higher variance. Figure 3 compares 50 Hz and 500 Hz recordings of the same programmed target translation of 18 counts (920 nm). The 50 Hz result demonstrates that multiple displacement/return movements were detectable over the movie duration but with a loss of fidelity, e.g. the detected movement of 998 nm that was more than 100 nm different from its corresponding return motion of 885 nm. The 500 Hz result appears much more precise but only captured a single displacement motion.

The clearest demonstration of noise improvement in 500 Hz recordings vs. 50 Hz recordings came from the fact that the minimum programmable target translation could be successfully identified only in the 500 Hz recordings, as seen in Figure 4. The 1 count motion was expected to be near 63.5 nm based on the stage motor's optical encoder resolution; this motion is well below the DH system's noise limit for 50 Hz holography. As such, the minimum target motion could not be discerned from the overall noise of 50 Hz recordings. However, the 500 Hz recording allowed the displacement to be clearly observed, and the mean surface phase results were within ~15 nm of the expected motion. This finding shows that the DH system should be able to detect the temporal phase change caused by <100 nm of average surface erosion during a 500 Hz recording. This is a key result indicating the possibility of successful *in situ* erosion detection of targets exposed to ET-arc plasma, though it should be noted that it is based on the assumption that temperature and vibrational effects would not significantly contribute to the frame-to-frame noise limit during a 1 ms shot.

A 3-D surface "warping" effect was observed in both 50 Hz and 500 Hz recordings (50 Hz example frames shown in Figure 5), which was another source of dynamic holographic noise. The holographic frames recording during translation events exhibited a distortion in flatness which changed frame-to-frame and was not a true representation

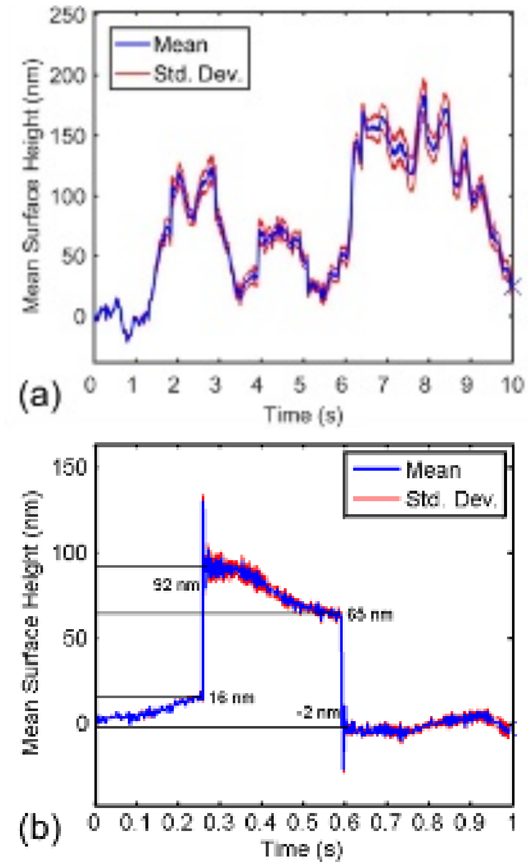

FIG. 4. (Color online). Motion detection of minimum programmable translation (1 count) from (a) 50 Hz and (b) 500 Hz recordings. Although three total displacement/return translations occurred in (a) from ~2 – 3 s, ~4 – 5 s, and ~6 – 8.5 s, the 50 Hz frame rate made the displacements undiscernible from noise. By contrast, in (b) the displacement and return could be clearly identified at 500 Hz.

of the actual object's rigid surface; that is, the holograms depicted dynamic surface warping as the surface displacement changed from its original position, but the actual object only experienced a change in displacement as the surface (a flat mirror) was static. This effect was apparent throughout the translation frames, but its severity seemed to be dependent on the instantaneous displacement away from the initial position. After completion of the translation event, the dynamic deformation ceased, but the displaced surface retained a high degree of anomalous warping in some cases. In recordings where the surface was returned from the displaced position to its initial position, the anomalous warping also disappeared. This behavior indicates that rapid displacement changes to a surface under observation, e.g. erosion of the full ROI, may introduce noise in the holograms occurring after the displacement change. The warping may result from wavefront mismatch of the object and reference beams, but more investigation is needed before any conclusive explanation can be made. Although ascertainment of the cause of this effect was not the focus of the present study, it will be important to understand for improvement of the DH diagnostic, and further exploration of the distortion and possible mitigation of it are relegated to future work.

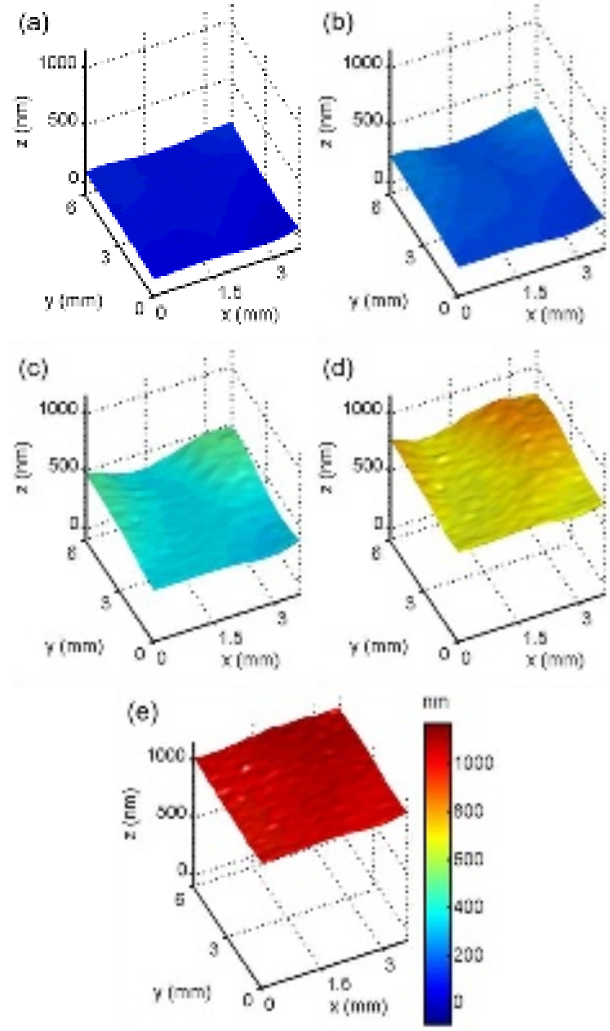

FIG. 5. (Color online). Anomalous holographic surface warping observed during ~1 μm translation recorded at 50 Hz, recorded at (a) t = 2.10 s, (b) t = 2.16 s, (c) t = 2.22 s, (d) t = 2.28 s, and (e) t = 2.34 s.

C. Dual Laser Holographic Motion Detection

Recordings of displacements from ~20 μm to ~400 μm were obtained via the DH system's dual laser mode. These translations were captured at a frame rate of 50 Hz only, because the translation stage's maximum speed could not produce the large displacements within the timeframe required for 500 Hz movies. The number of frames per recording was raised to 700 for some cases in order to allow the largest programmed translations to be performed within the duration of a single movie. This resulted in movies with a total elapsed time of up to 14 s. Additionally, since a dual laser hologram is produced by subtraction of a single laser hologram from another single laser hologram, the analyzed dual laser frames were 350 in total and separated by 4 ms rather than 2 ms to account for the subtraction of adjacent frames.

Similar to the single laser movies, noise from various sources affected dual laser recordings. The synthetic wavelength factor of ~440 not only measures true surface variations observed in a hologram up to the expanded 2π range but also multiplies noise in the hologram by the same degree. This effectively means that a dual laser holographic phase image has a lower limit of discernable surface variation in the z-axis of ~100 µm.[7]

The movie technique demonstrated in this work allows this limit to be lowered dramatically if the surface variation of interest can be dynamically recorded. While a dual laser phase image generated by two single laser holograms captured out of sequence (i.e. with several seconds or minutes of elapsed time between them) cannot be resolved in the z-axis below ~100 µm, frame-to-frame noise in a flatfield corrected 50 Hz dual laser movie is typically ~5 µm. The drawback is that any static surface features that were present before the movie began are not captured since subtraction of the initial frame from all subsequent frames leaves a "flat" hologram throughout. However, a surface variation dynamically appearing within the duration of the movie can be captured and discerned by comparing the surface heights before and after the event, with a projected z-axis resolution limit of ~20 µm.

The dual laser movies include an anomaly that was not observed in the single laser movies. Large displacements with significant frame-to-frame variation were exhibited during translation events as shown in Figure 6.a; the translation event occurred from t = ~2.5 s to 6 s and is shaded in gray. The detected motion during this time appeared to be hundreds of µm in the opposite direction of programmed translation. However, the detected mean surface height after motion ceased was stable around 47 µm (t = 6 s to 10 s). This value was within 10 µm of the expected

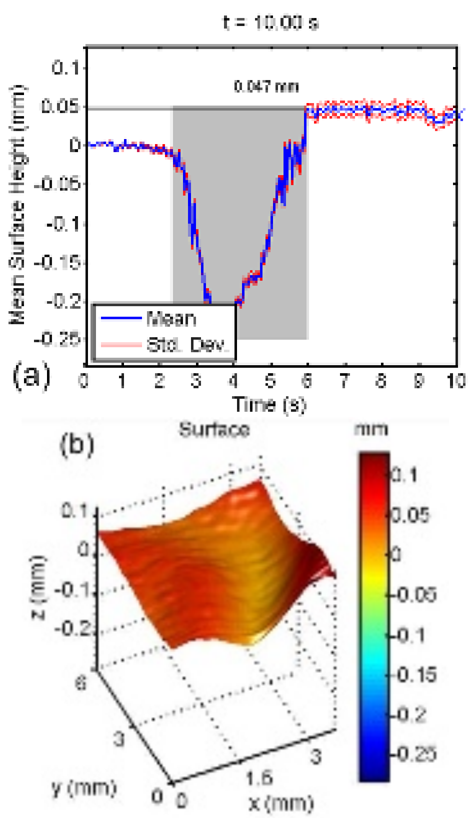

FIG. 6. (Color online). (a) Detected motion of 880 counts translation from a 50 Hz dual laser recording. (b) The 3-D phase image for t = 10 s.

displacement. Therefore, the detected surface heights before and after the translation events were reproducible and relatively accurate.

The 3-D surface warping effect observed in the single laser results was also present in the dual laser recordings. The phase image of Figure 6.b shows ~150 µm of flatness distortion after a programmed translation equivalent to 56 µm. The warping effect could potentially complicate detailed analyses such as depth of individual surface features apparent after erosion. The warping effect was generally less pronounced when the programmed translation was larger as exemplified by Figure 7. The detected mean surface height after translation was 256 µm, but the associated phase image exhibited flatness distortion of ~100 µm. This phase image noise was therefore not observed to increase as the size of the surface displacement was increased, which followed typical dual laser surface noise behavior.

The detected final surface heights post-translation are tabulated in Table II. Despite the noise from the target motion and the 3-D phase image warp, the results are remarkably close to the expected final target positions based on a programmed translation increment of 63.5 nm per count (note that the manufacturer's quoted resolution is used in the calculation of the programmed translated height since the displacements far exceeded the actuator's bi-directional repeatability of ±1 µm). The results were repeated at each programmed translation size to demonstrate reproducibility. Figure 8 provides plots of the

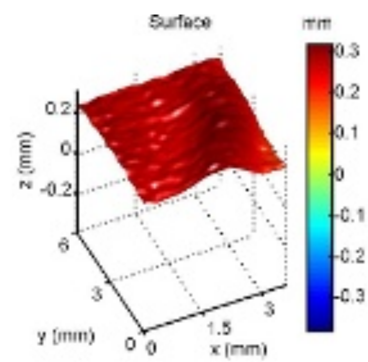

FIG. 7. (Color online). 3-D phase image after 256 µm translation.

TABLE II. Dual Laser DH Detected Motion.

Translation (Counts)	50 Hz Detected Surface Height (µm), Group 1	500 Hz Detected Surface Height (µm), Group 2	Programmed Translated Height (µm), 63.5 nm Per Count
440	43	47	28
880	50	47	56
1,320	82	83	84
1,760	121	84	112
2,000	135	132	127
3,000	202	197	191
4,000	268	256	254
5,000	304	313	318
6,000	391	374	381

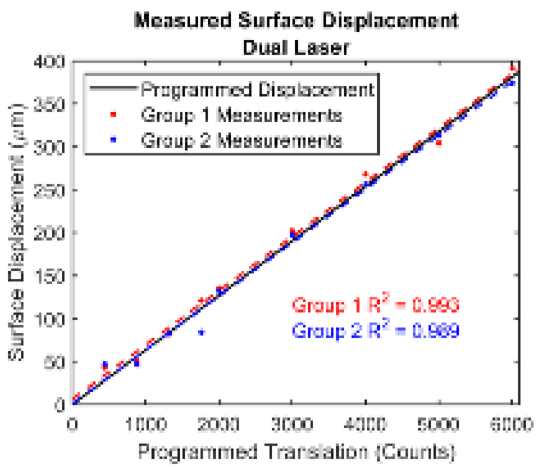

FIG. 8. (Color online). Dual laser DH detected motion vs. programmed translation.

expected and detected surface heights, and the high linearity of the detected results is seen in the R^2 values of 0.99 for both data groups.

D. Proof-of-principle *In Situ* Demonstration

The *in situ* plasma erosion measurement demonstration experiment plan involved the use of a 304 stainless steel target configuration similar to the *ex situ* characterization target, with an increased thickness for the cover plate which produced a shadowed region substantial enough to act as a fiducial. The target base plate width and height were both 7.62 cm, and the cover plate dimensions were 3.19 x 1.91 cm; both the base and cover plate depths were 635 mm. The target had an initial mirror-like finish with a roughness average (Ra) of 10 nm. Figure 9.a shows the pristine target with excellent reflectivity of the ceiling light and other overhead objects, and 9.b shows its plasma-exposed surface in which the fiducial region is visible, with overlays of the approximate DH field of view and cropped 6.3 x 14.4 mm ROI corresponding to the example phase image of Figure 9.c.

Noise levels for the *in situ* experiment were higher than in the benchtop characterization configuration due to the increased optical path length for the DH lasers and increased vibration in the surroundings from the ET-arc components. A position FFT from an accelerometer measurement of the ET-arc chamber recorded during a plasma event is shown in Figure 10. Low frequency noise on the order of 1 to 100 µm was measured, while noise at higher frequencies reached amplitudes of ~10 nm. In practice, low frequency noise would occur over several milliseconds and could therefore be mitigated by selecting only the subsequent frames of interest surrounding a plasma event during *in situ* recordings, although the high frequency noise was anticipated to indicate that interframe noise for *in situ* plasma recordings would be higher than the levels observed in the translation stage recordings.

Single laser holographic recordings were made at 500 Hz which captured the target surface before, during, and

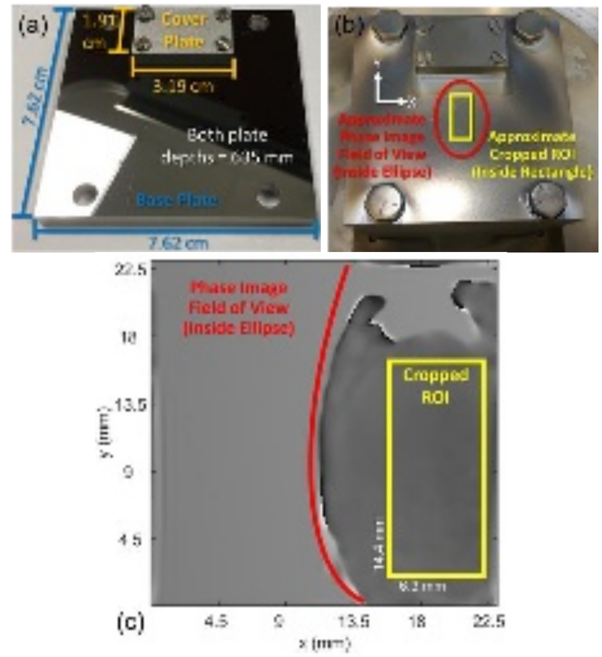

FIG. 9. (Color online). Pristine *in situ* demonstration target (a) and its plasma-exposed surface with overlays of the approximate DH field of view in red and cropped ROI in yellow (b), with corresponding example phase image (c).

after plasma events. Additionally, single-frame holograms were recorded under quiescent conditions before and after each plasma exposure. A total of 10 plasma exposures were conducted while the holographic ROI was centered on the plasma strike zone with the shadowed region just out of frame. A second set of 10 additional plasma exposures was conducted after the ROI was changed to center on the shadowed region. Figure 11 shows the detected surface elevation change during two plasma events. Analysis was performed by subtracting a frame captured just before the plasma shot from all other frames in the sequence so that the surface zero-position would be temporally adjacent to the plasma event. The plasma strike in Figure 11.a occurred at 606 ms into the recording. The vibrational noise can be seen in the figure in the form of large low-frequency motion prior to the plasma shot. Immediately following the plasma event, major vibration was observed for ~50 ms, and afterward the surface retained an elevated height compared to its pre-plasma position. Figure 11.b shows a longer duration

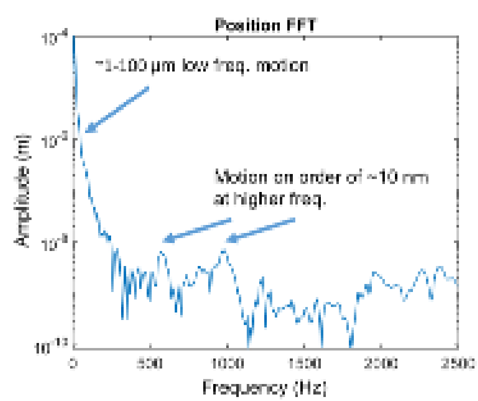

FIG. 10. (Color online). Noise levels from an ET-arc plasma shot.

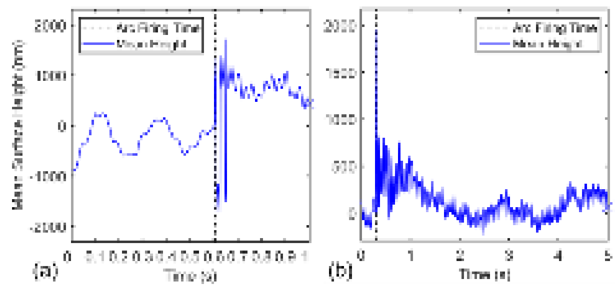

FIG. 11. (Color online). Dynamic surface change detected during a 1-second 500 Hz recording of an ET-arc plasma event (a) and a 5-second 500 Hz recording of another plasma event (b).

recording in which the plasma shot occurred 298 ms after the recording began; the initial large vibration was again seen immediately after the plasma shot, and the elevated post-plasma position was shown to gradually decrease over ~2 s until it returned to the initial level. The large vibration and elevated post-plasma surface were consistent with expected plasma thrust and thermal expansion of the target surface which had been predicted in previous work.[8]

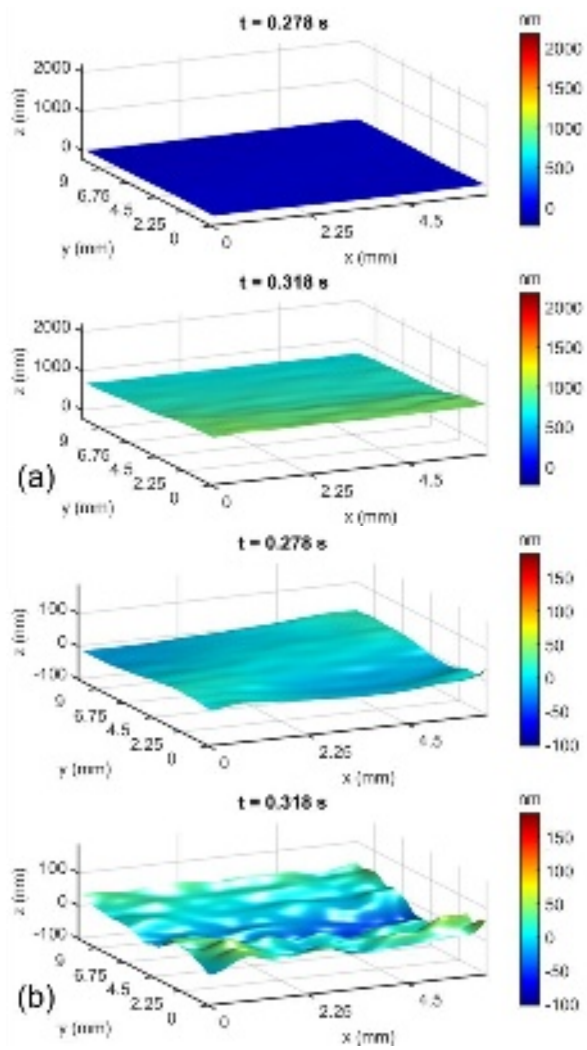

FIG. 12. (Color online). Selected surface renderings captured 20 ms before (t = 0.278 s)) and after (t = 0.318 s) the plasma event in the recorded sequence of Fig. 11.b. (a) Surfaces including overall elevation from plasma thrust and thermal effects. (b) The same surfaces with elevation removed.

The surface data was normalized to the shadowed region in the holograms which served as the fiducial. Surface elevation was removed from the frame sequence by subtracting the difference of each frame's mean surface height in the fiducial region from the first frame's mean height of the same area. The effect of this is shown in Figure 12, where selected normalized surfaces from a sequence clearly show the surface erosion in detail with overall elevation removed and scaling tightened. The measured erosion depth is 50–100 nm.

Selected single-frame phase renderings are shown in Figure 13; the holograms used in Figure 13.a were taken during the first 10 plasma exposures, and those of Figure 13.b were taken during 10 additional plasma exposures. Each hologram has been flatfield corrected with a hologram of the surface prior to new plasma exposures. Note that this means the surfaces in Figure 13.b already had erosion from the first 10 plasma exposures, but that pre-existing surface erosion was subtracting leaving only the new erosion from the additional 10 exposures. In Figure 13.a, the holographic ROI was centered on the plasma strike zone, and an overall depression was observed to form at that position on the target over the course of the repeated plasma exposures, although only to a depth of a few hundred nm. Fine surface features generally changed with each new plasma strike. These results are likely to be affected by single-frame image noise, but redeposition in the plasma strike zone is known to occur from the *ex situ* characterization[12] and therefore the relatively subtle surface changes in these images are not unexpected. In Figure 13.b, the ROI was centered on the fiducial (which was situated in the area of y > ~8 mm), and a trench formation similar to that which was observed in the *ex situ* characterization experiments could be seen. The y-

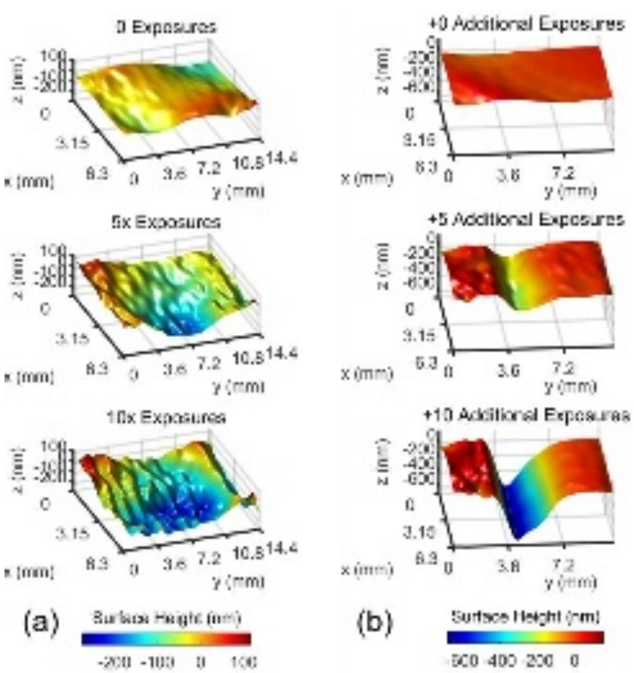

FIG. 13. (Color online). Selected single-frame holograms for (a) the first 10 plasma exposures with an ROI centered on the plasma strike zone and (b) 10 additional plasma exposures with the ROI changed to encompass the fiducial region.

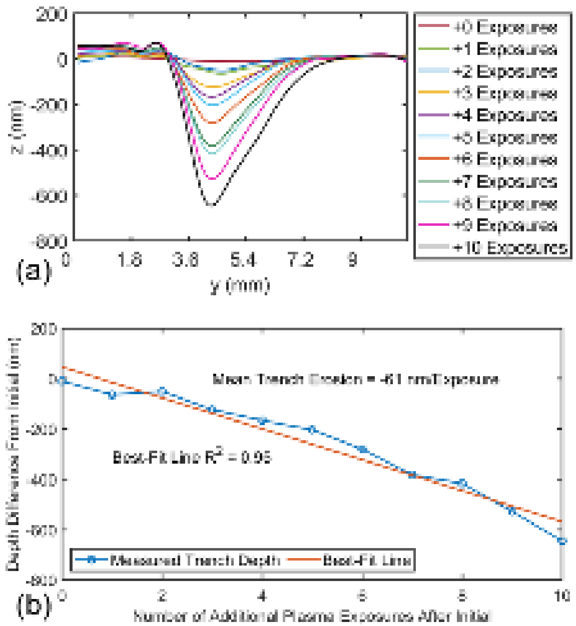

FIG. 14. (Color online). Surface height profiles (a) and mean erosion (b) for the 10 additional plasma exposures after the first 10 were completed.

axis surface profiles with height averaged along the x-axis for Figure 13.b are given in Figure 14. The trench formation steadily deepened with repeated plasma exposures, and analysis of the minima of the line profiles revealed a highly linear trend with an average erosion in the trench of 61 nm per plasma shot. This finding agreed with the measured erosion from the *in situ* recording of Figure 12, as well as the expectation from the *ex situ* characterization that the inclusion of a cover plate on the target would produce progressive trench-like plasma erosion.

V. SUMMARY

The ORNL digital holography diagnostic for measuring 3-D surface deformation was characterized *ex situ* on targets exposed to plasma from an electrothermal arc, and measurements of ~150 nm of erosion per plasma shot were obtained. Recordings of a moving mirror target mounted on a precision electronic translation stage were made at 50 Hz and 500 Hz in single laser mode, and 50 Hz in dual laser mode. These recordings showed the ability of the holography system to measure dynamic displacements of the overall ROI with good accuracy and reduced frame-to-frame noise on the order of tens of nm in single laser mode and tens of μm in dual laser mode. These findings along with the successful *ex situ* erosion measurements indicated that the diagnostic could be coupled with the electrothermal arc for an *in situ* demonstration. Results of that demonstration showed the ability of digital holography to successfully detect surface changes before, during, and after ET-arc plasma events, and progressive trench-like erosion of 61 nm per plasma shot was observed. The DH system under the configuration for *in situ* measurements on the ET-arc could be used for potential future experiments such as characterizing the ET-arc plasma alongside other plasma diagnostics, ascertaining the physical process which produces the trench-like erosion, and conducting a robust PMI campaign with fusion-relevant materials and geometries. Improving the understanding and mitigation of errors such as anomalous surface distortion and vibrational noise are among future developmental goals leading towards potential deployment in a more challenging PMI research facility such as ORNL's Material Plasma Exposure Experiment (MPEX).

VI. ACKNOWLEDGMENTS

This manuscript has been authored by UT-Battelle, LLC, under contract DE-AC05-00OR22725 with the US Department of Energy (DOE). The US government retains and the publisher, by accepting the article for publication, acknowledges that the US government retains a nonexclusive, paid-up, irrevocable, worldwide license to publish or reproduce the published form of this manuscript, or allow others to do so, for US government purposes. DOE will provide public access to these results of federally sponsored research in accordance with the DOE Public Access Plan (http://energy.gov/downloads/doe-public-access-plan).

AIP PUBLISHING DATA SHARING POLICY

The data that support the findings of this study are available from the corresponding author upon reasonable request.

VII. REFERENCES

[1]G. Federici *et al.*, Jour. Nuc. Mat. **313-136**, pp. 11-22 (2003).
[2]A. Kreter, Fusion Sci. & Tech. **59**, 1T (2011).
[3]G. Pedrini, I. Alekseenko, G. Jagannathan, M. Kempenaars, G. Vayakis, and W. Osten, Appl. Optics **58** (5), pp. A147-A155 (2019).
[4]C. E. Thomas, E. M. Granstedt, T. M. Biewer, L. R. Baylor, S. K. Combs, S. J. Meitner, D. L. Hillis, R. Majeski, and R. Kaita, Rev. Sci. Instrum. **85**, 11D810 (2014).
[5]C. E. Thomas *et al.*, Rev. Sci. Instrum. **87**, 11D624 (2016).
[6]T. M. Biewer, J. C. Sawyer, C. D. Smith, and C. E. Thomas, Rev. Sci. Instrum. **89**, 10J123 (2018).
[7]C. D. Smith, T. M. Biewer, X. Ren, C. E. Thomas, T. Gebhart, and Z. Zhang, Trans. Plasma Sci., Online (2019).
[8]T. M. Biewer, C. D. Smith, T. E. Gebhart, A. Greenhalgh, X. Ren, and C. E. Thomas, Jour. Instrum. 15, C02017 (2020).
[9]T. E. Gebhart, L. R. Baylor, J. Rapp, and A. L. Winfrey, Jour. Appl. Phys. 123, 033301 (2018).
[10]C. D. Smith, Ph. D. diss., University of Tennessee (2020).
[11]E. G. Lindquist, T. E. Gebhart, D. Elliott, Z. He, N. Kafle, C. D. Smith, C. E. Thomas, S. J. Zinkle, and T. M. Biewer, Fusion Sci. & Tech. (submitted Nov. 2020).
[12]C. D. Smith, T. M. Biewer, T. Gebhart, J. Echols, and C. E. Thomas, Rev. Sci. Instrum. (submitted Dec. 2020).

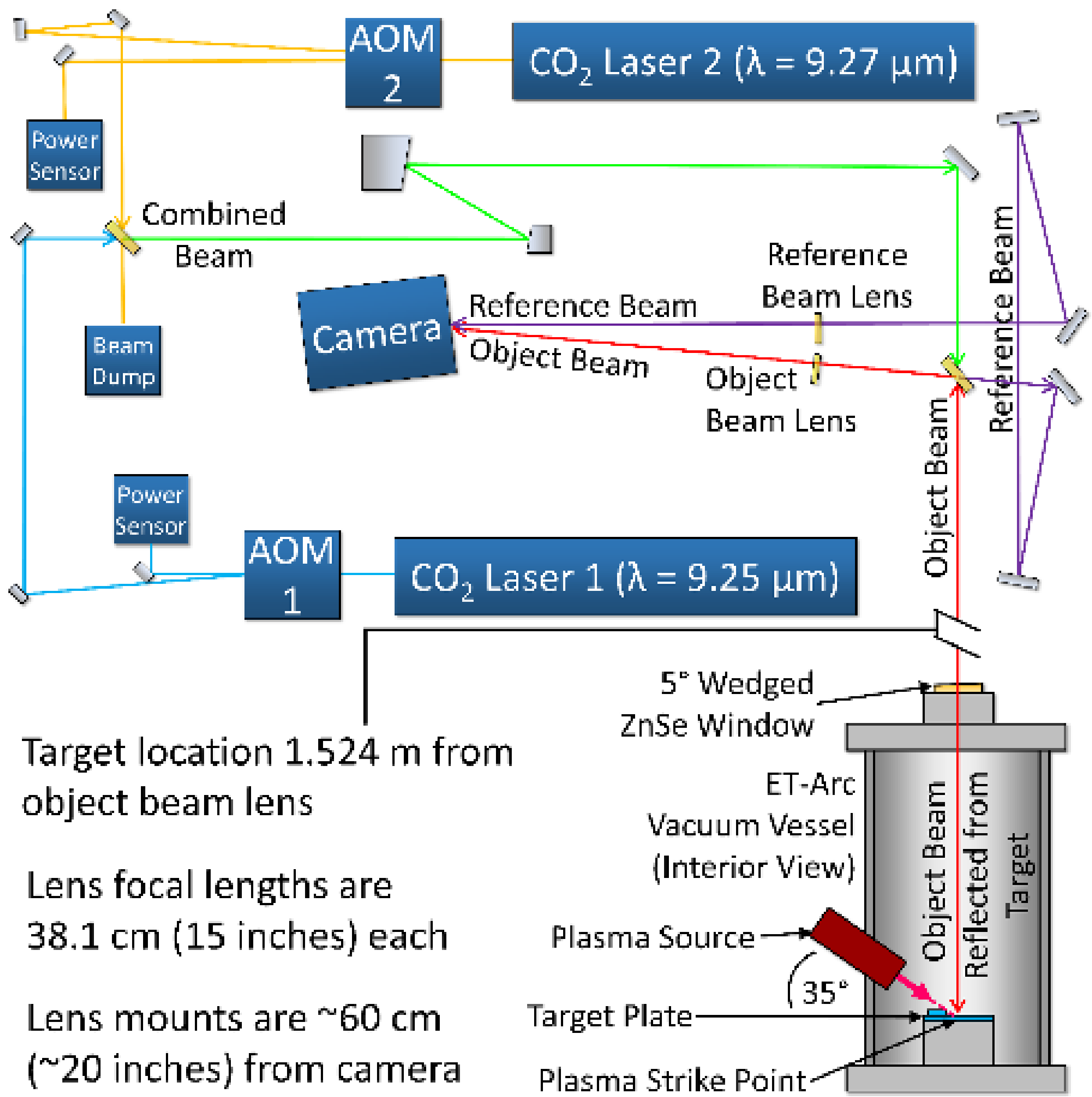
AOM 2
CO2 Laser 2 (λ = 9.27 µm)
Power Sensor
Combined Beam
Beam Dump
Reference Beam Lens
Camera
Reference Beam
Object Beam
Object Beam Lens
Reference Beam
Object Beam
Power Sensor
AOM 1
CO2 Laser 1 (λ = 9.25 µm)
5° Wedged ZnSe Window
Target location 1.524 m from object beam lens
Lens focal lengths are 38.1 cm (15 inches) each
Lens mounts are ~60 cm (~20 inches) from camera
ET-Arc Vacuum Vessel (Interior View)
Object Beam Reflected from Target
Plasma Source
35°
Target Plate
Plasma Strike Point

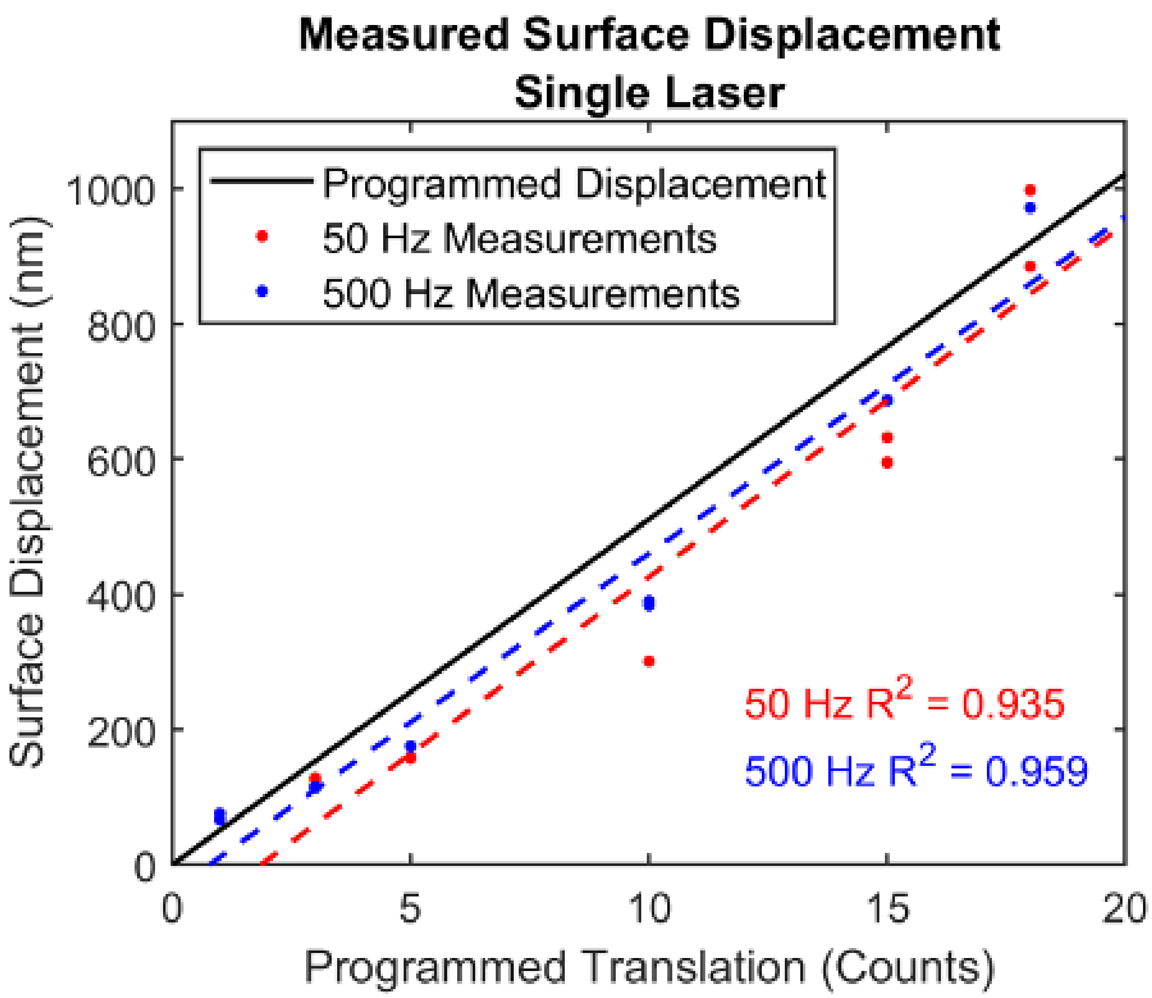
Measured Surface Displacement
Single Laser
Programmed Displacement
50 Hz Measurements
500 Hz Measurements
50 Hz R2 = 0.935
500 Hz R2 = 0.959
Surface Displacement (nm)
Programmed Translation (Counts)
0
200
400
600
800
1000
0
5
10
15
20

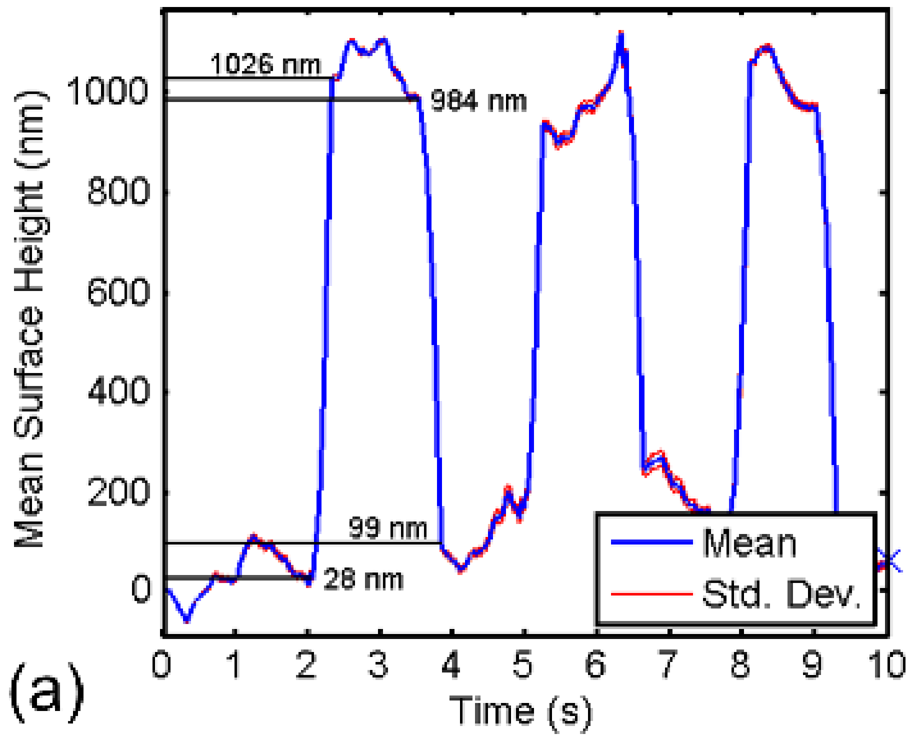
1026 nm
984 nm
99 nm
28 nm
Mean
Std. Dev.
Mean Surface Height (nm)
Time (s)
(a)

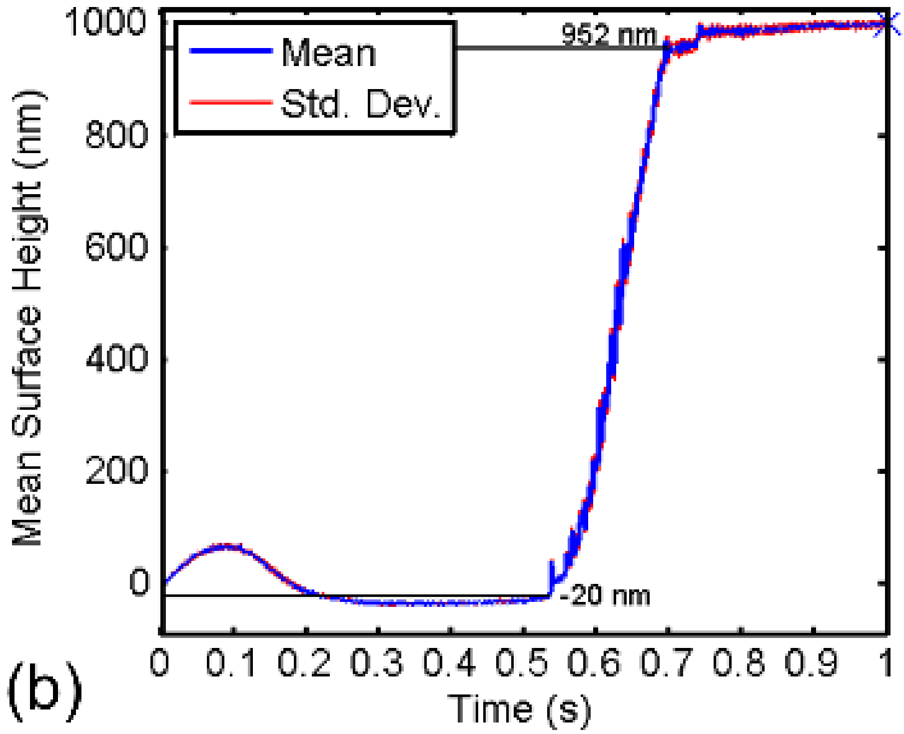
Mean
Std. Dev.
952 nm
-20 nm
Mean Surface Height (nm)
1000
800
600
400
200
0
0
0.1
0.2
0.3
0.4
0.5
0.6
0.7
0.8
0.9
1
Time (s)
(b)

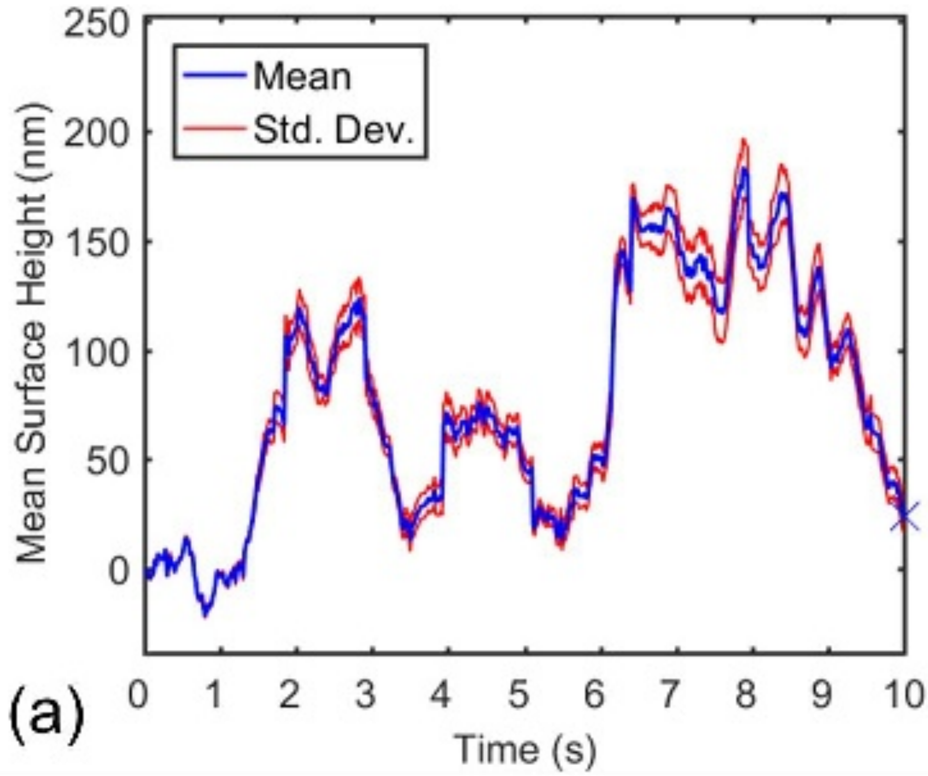
Mean
Std. Dev.
Mean Surface Height (nm)
250
200
150
100
50
0
0 1 2 3 4 5 6 7 8 9 10
Time (s)
(a)

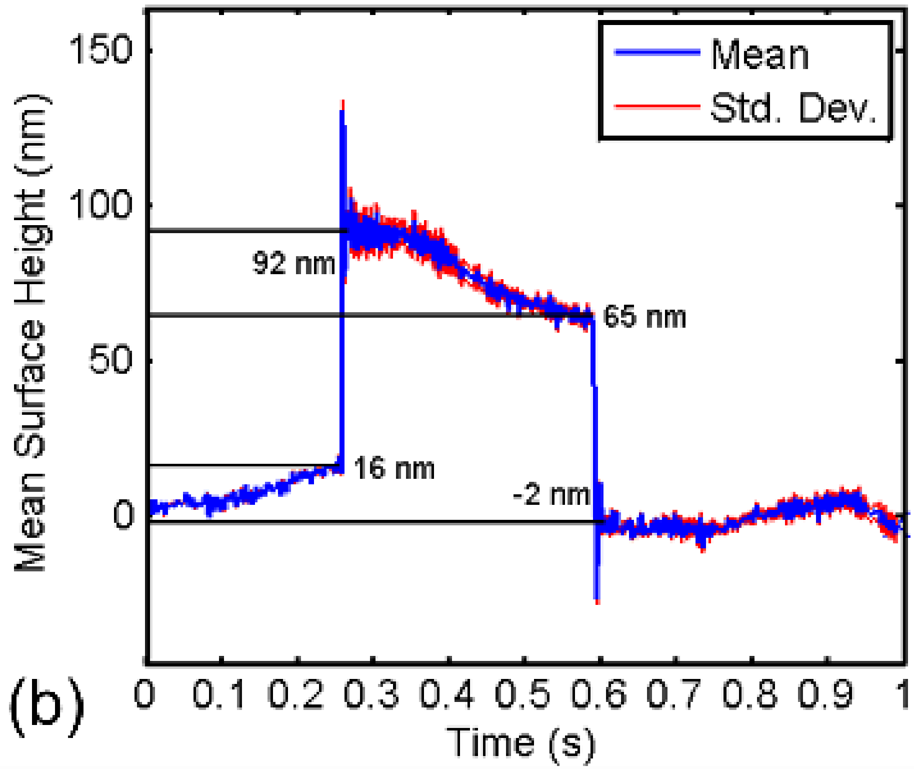
Mean
Std. Dev.
92 nm
65 nm
16 nm
-2 nm
Mean Surface Height (nm)
150
100
50
0
(b)
0 0.1 0.2 0.3 0.4 0.5 0.6 0.7 0.8 0.9 1
Time (s)

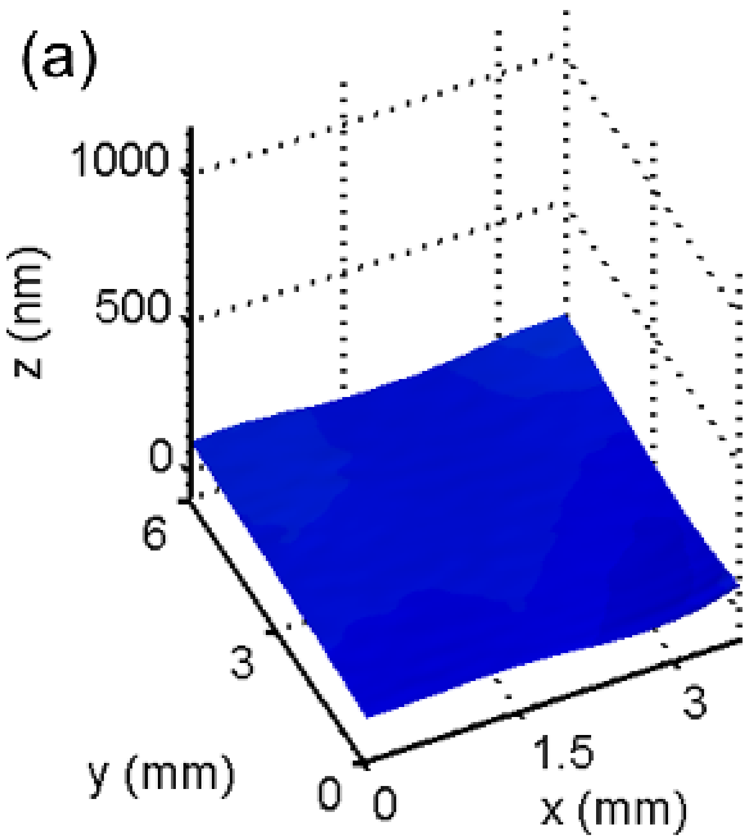
(a)
1000
500
0
z (nm)
6
3
0
y (mm)
0
1.5
3
x (mm)

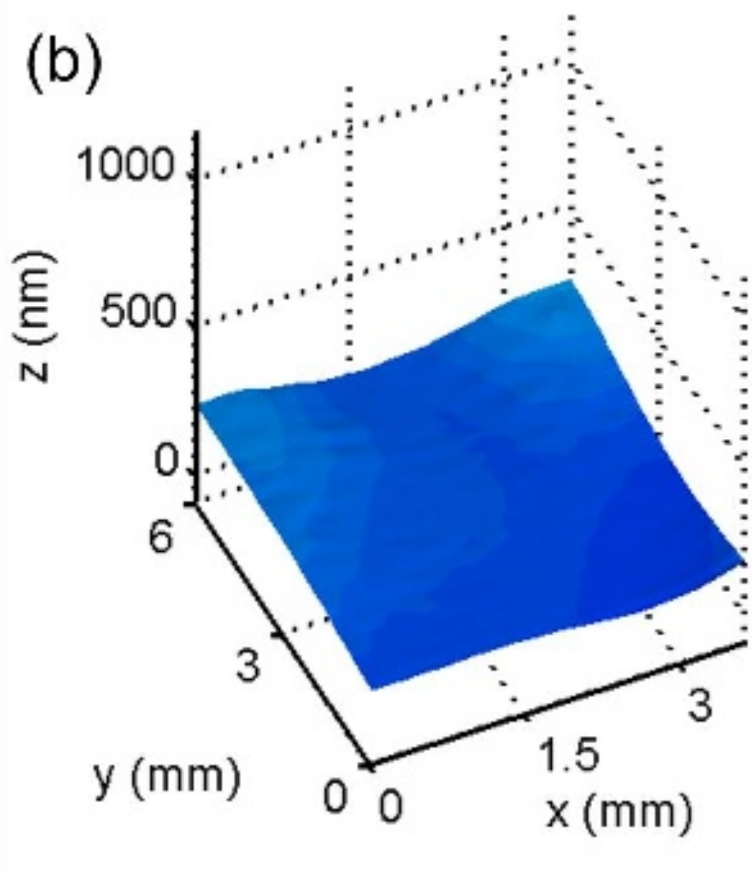
(b)
z (nm)
1000
500
0
6
3
y (mm)
0
0
1.5
3
x (mm)

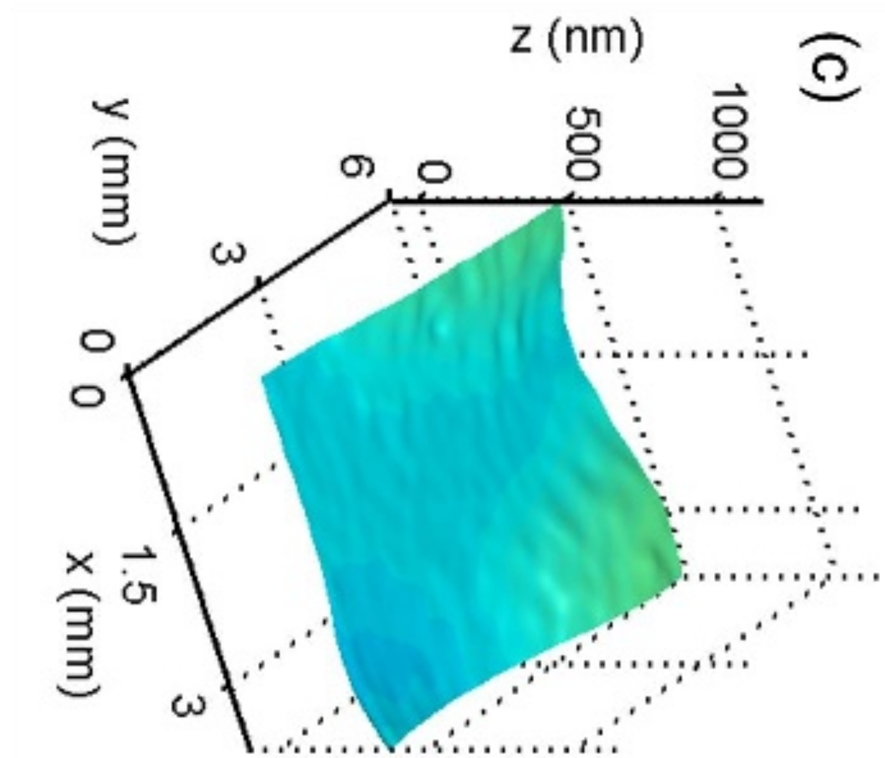
(c)
z (nm)
1000
500
0
6
3
y (mm)
0
0
1.5
3
x (mm)

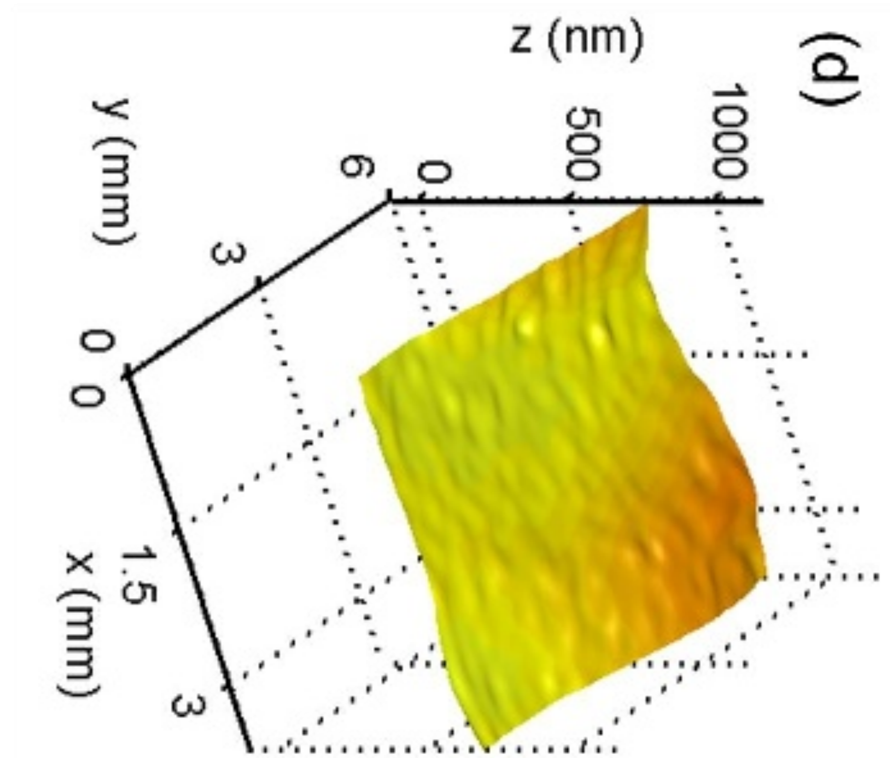
(d)
z (nm)
1000
500
0
6
3
0
y (mm)
0
1.5
3
x (mm)

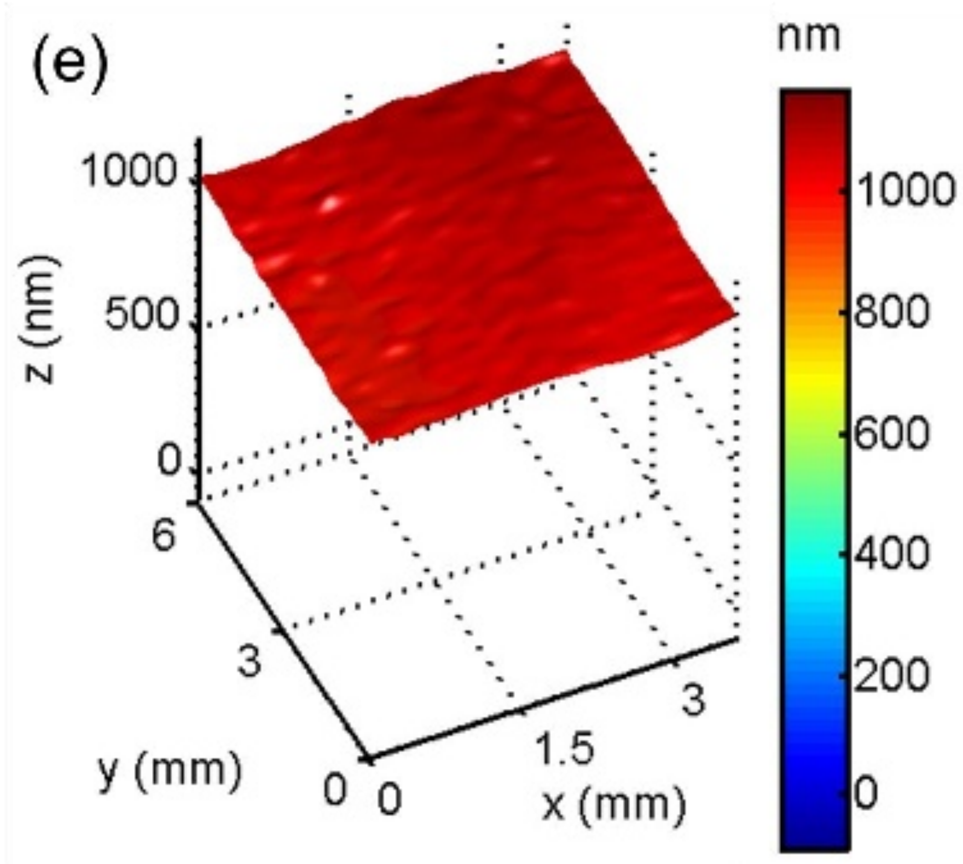
(e)
nm
1000
500
0
z (nm)
6
3
0
y (mm)
0
1.5
3
x (mm)
1000
800
600
400
200
0

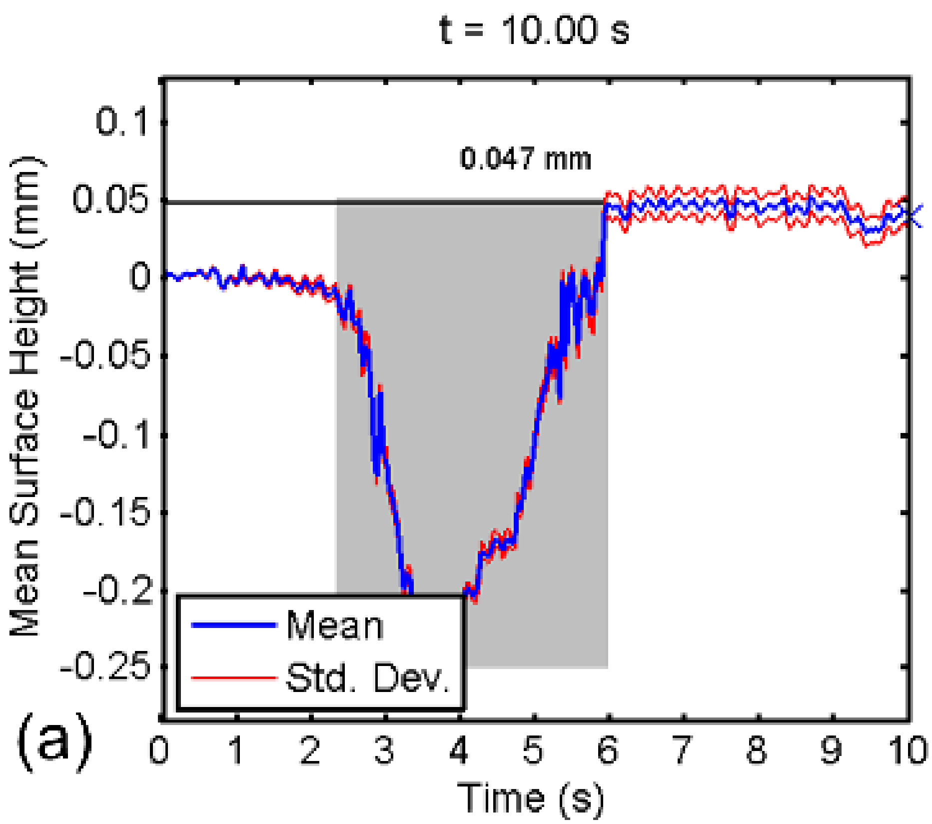
t = 10.00 s
0.047 mm
Mean Surface Height (mm)
0.1
0.05
0
-0.05
-0.1
-0.15
-0.2
-0.25
Mean
Std. Dev.
(a)
0
1
2
3
4
5
6
7
8
9
10
Time (s)

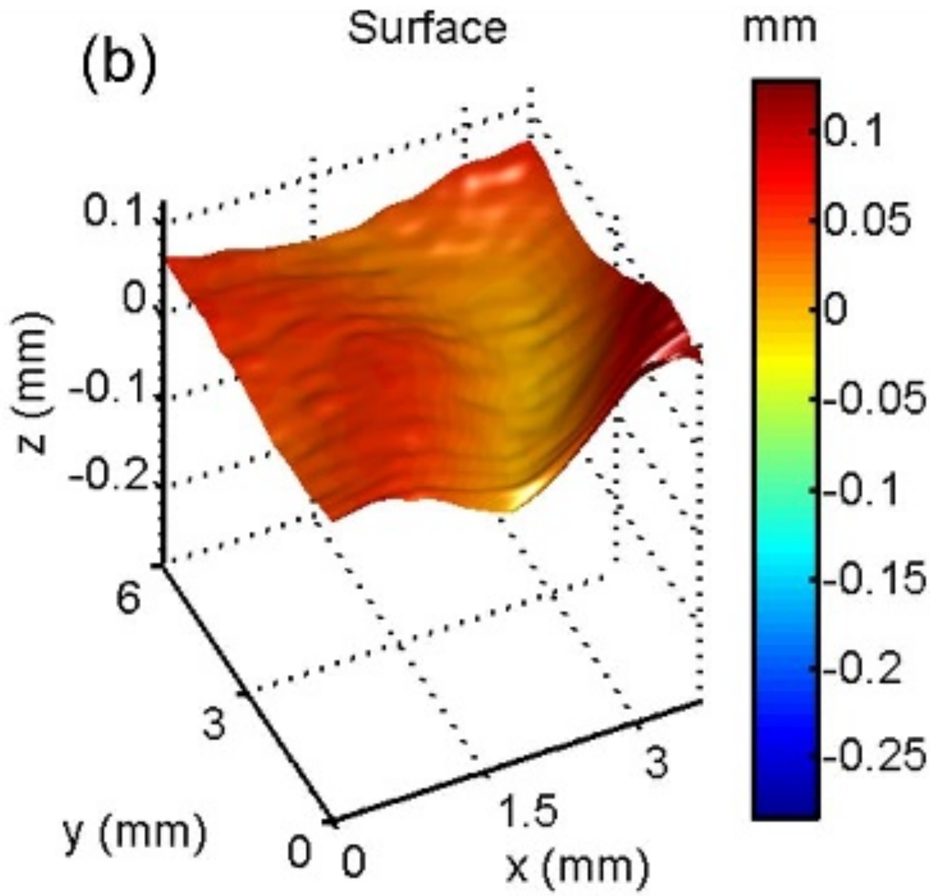
(b)
Surface
mm
0.1
0
-0.1
-0.2
z (mm)
6
3
0
y (mm)
0
1.5
3
x (mm)
0.1
0.05
0
-0.05
-0.1
-0.15
-0.2
-0.25

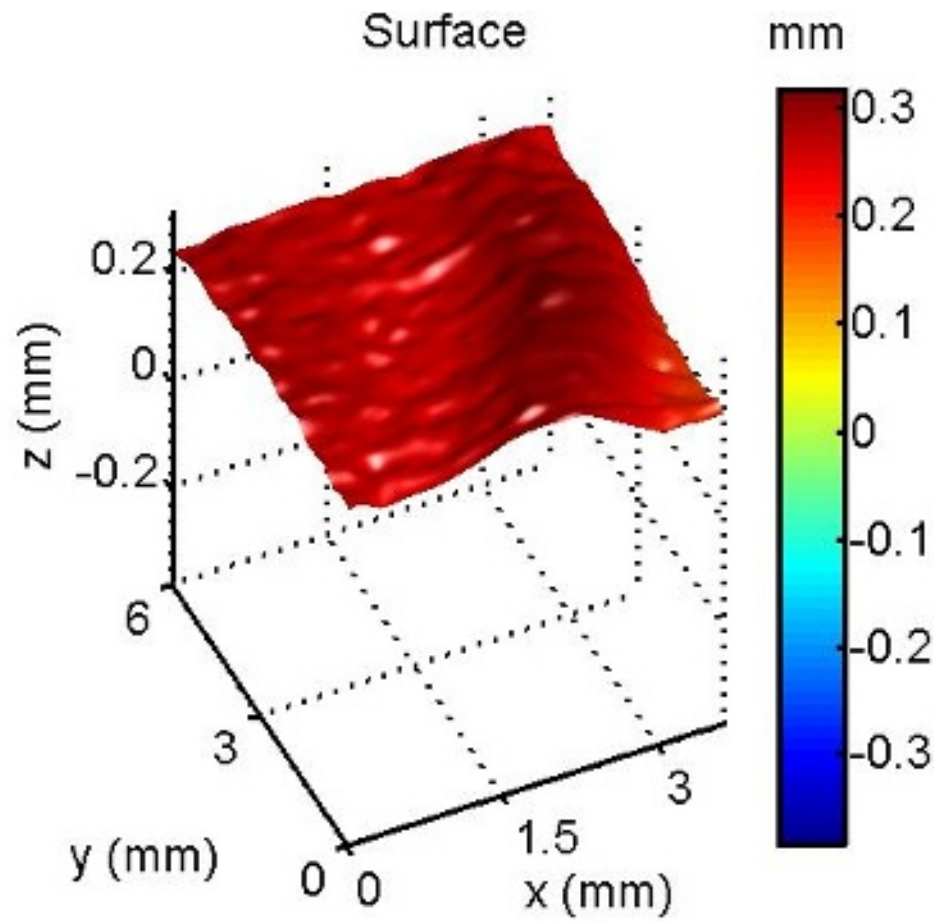
Surface
mm
0.3
0.2
0.1
0
-0.1
-0.2
-0.3
z (mm)
0.2
0
-0.2
6
3
0
y (mm)
0
1.5
3
x (mm)

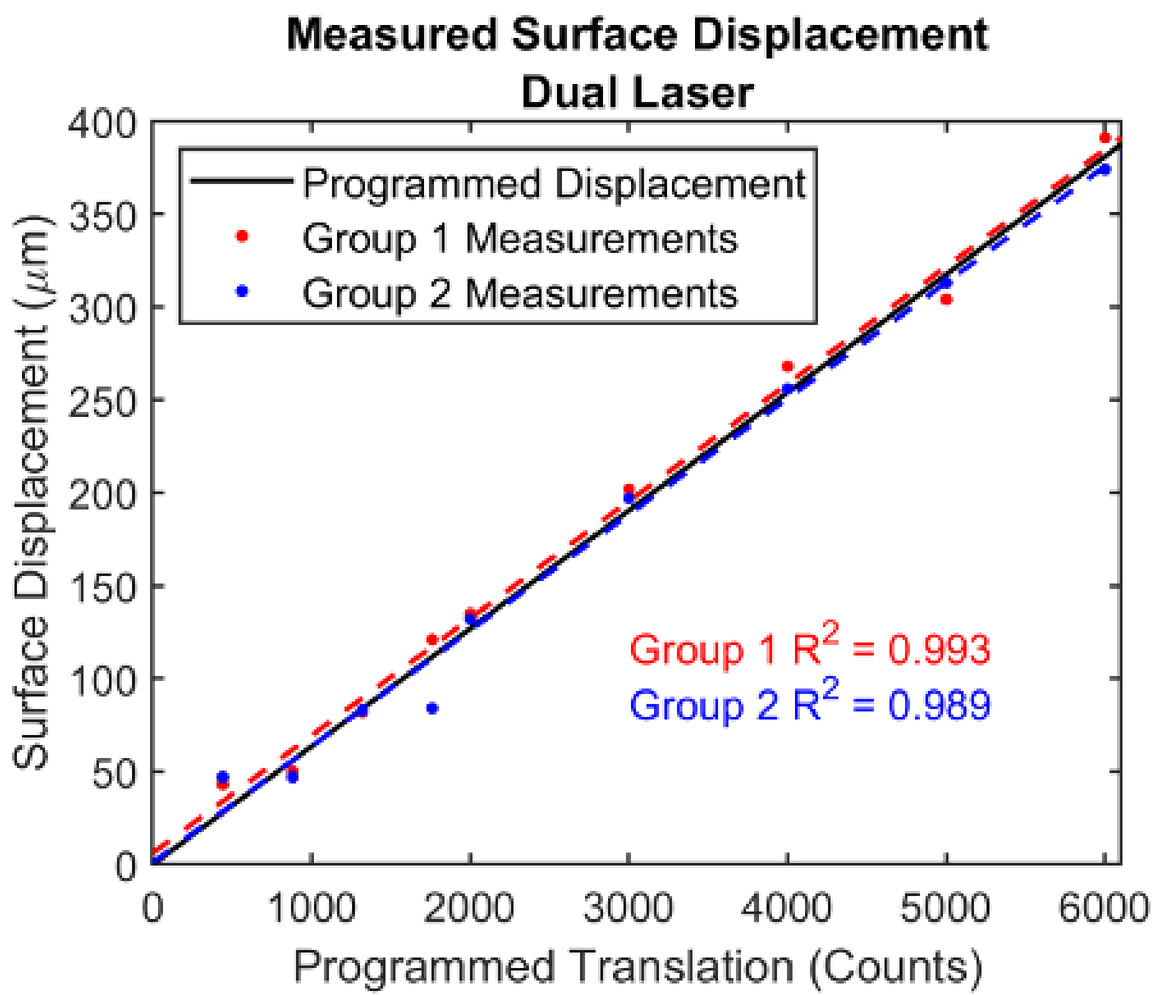
Measured Surface Displacement
Dual Laser
Surface Displacement (μm)
Programmed Translation (Counts)
Programmed Displacement
Group 1 Measurements
Group 2 Measurements
Group 1 R2 = 0.993
Group 2 R2 = 0.989
0
50
100
150
200
250
300
350
400
0
1000
2000
3000
4000
5000
6000

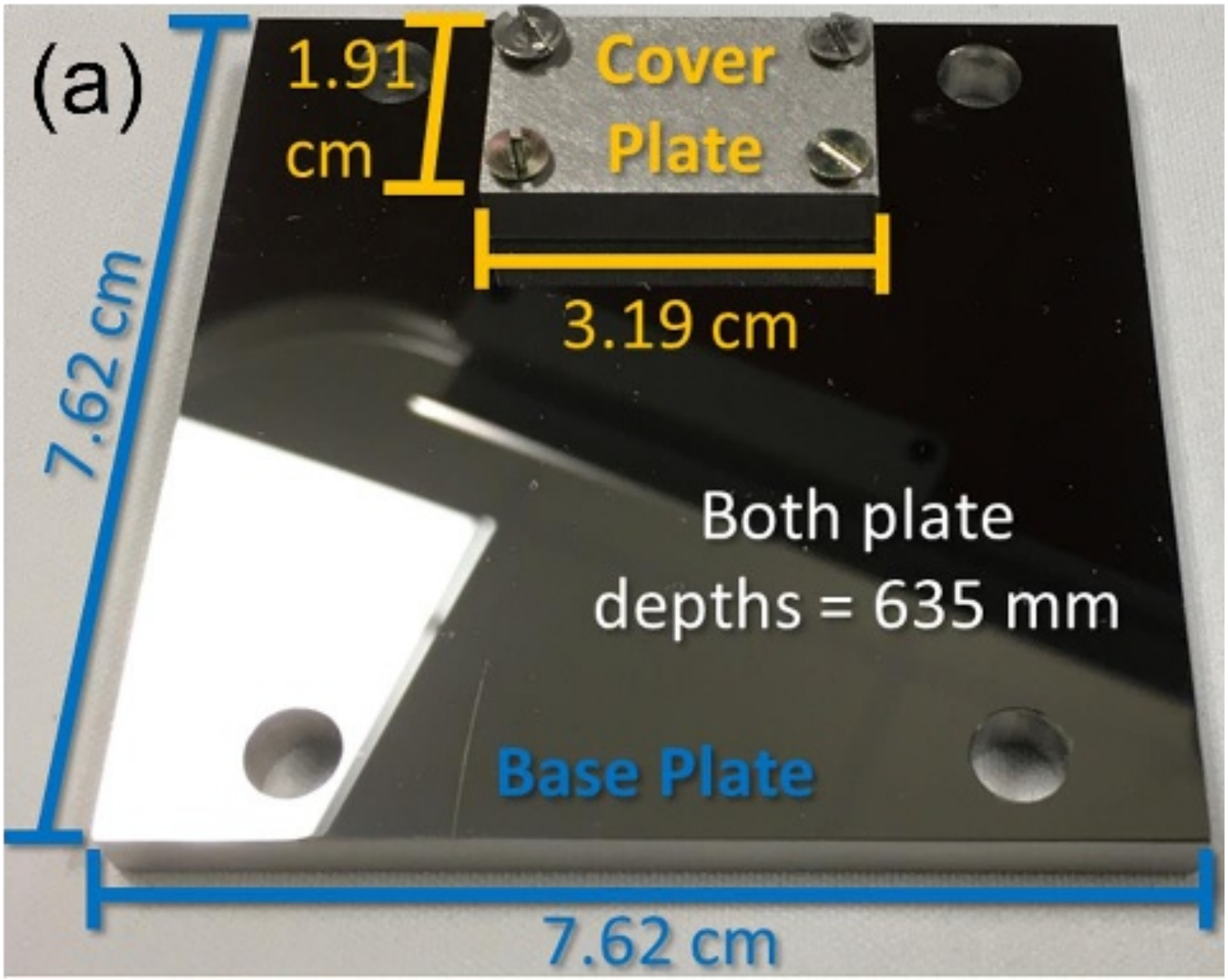
(a)
1.91 cm
Cover Plate
3.19 cm
7.62 cm
Both plate depths = 635 mm
Base Plate
7.62 cm

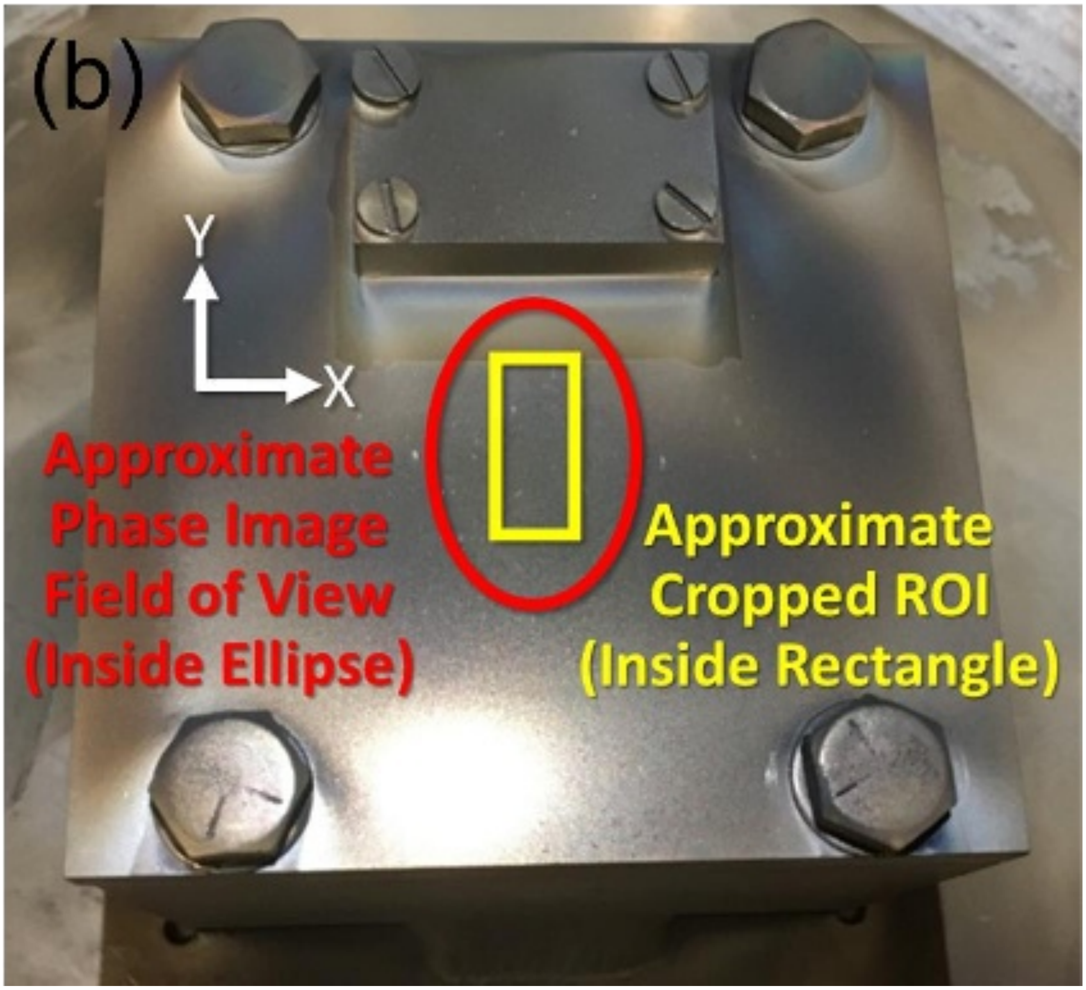
(b)
Y
X
Approximate
Phase Image
Field of View
(Inside Ellipse)
Approximate
Cropped ROI
(Inside Rectangle)

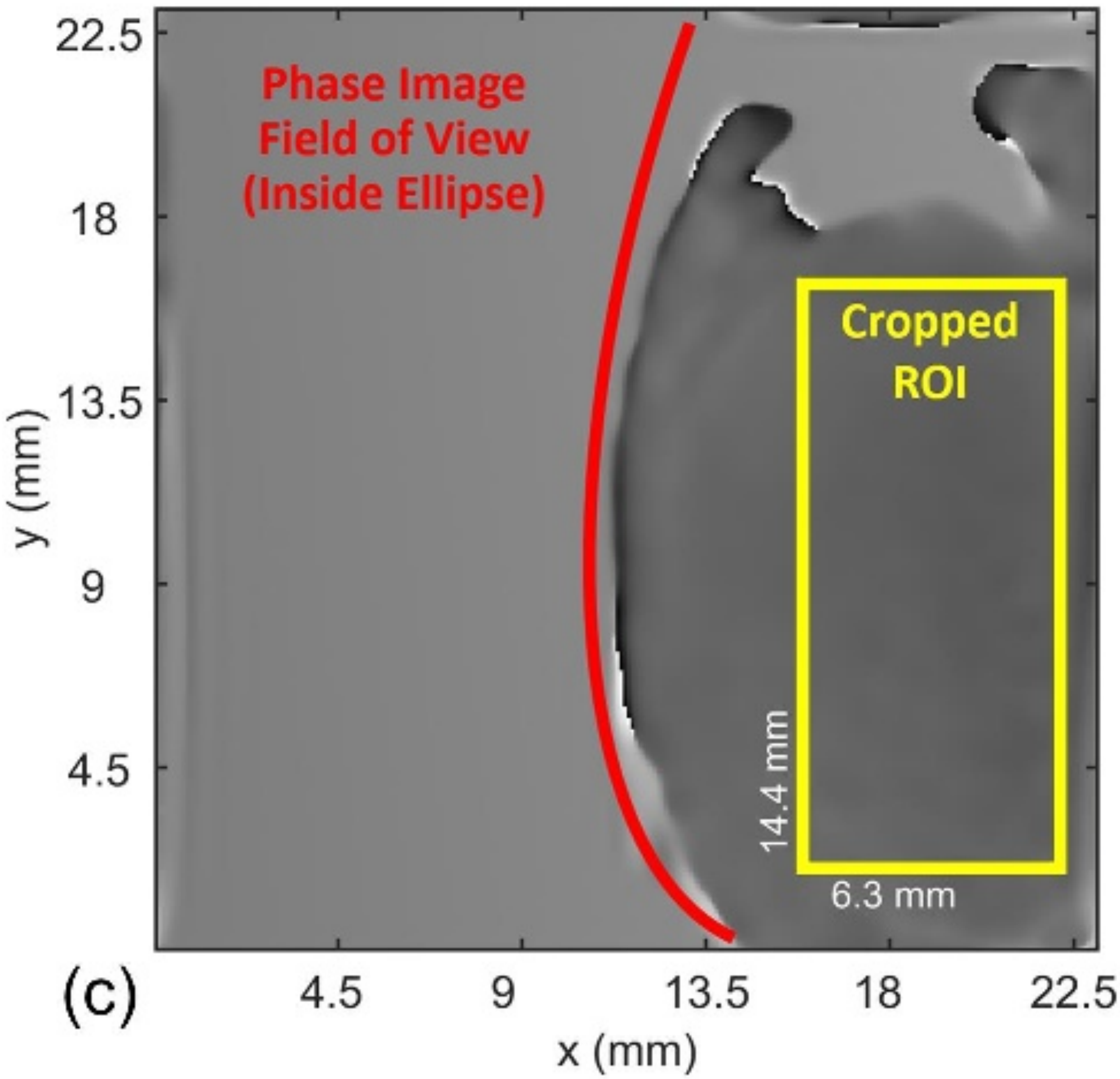
22.5
18
13.5
9
4.5
y (mm)
Phase Image
Field of View
(Inside Ellipse)
Cropped
ROI
14.4 mm
6.3 mm
4.5
9
13.5
18
22.5
x (mm)
(c)

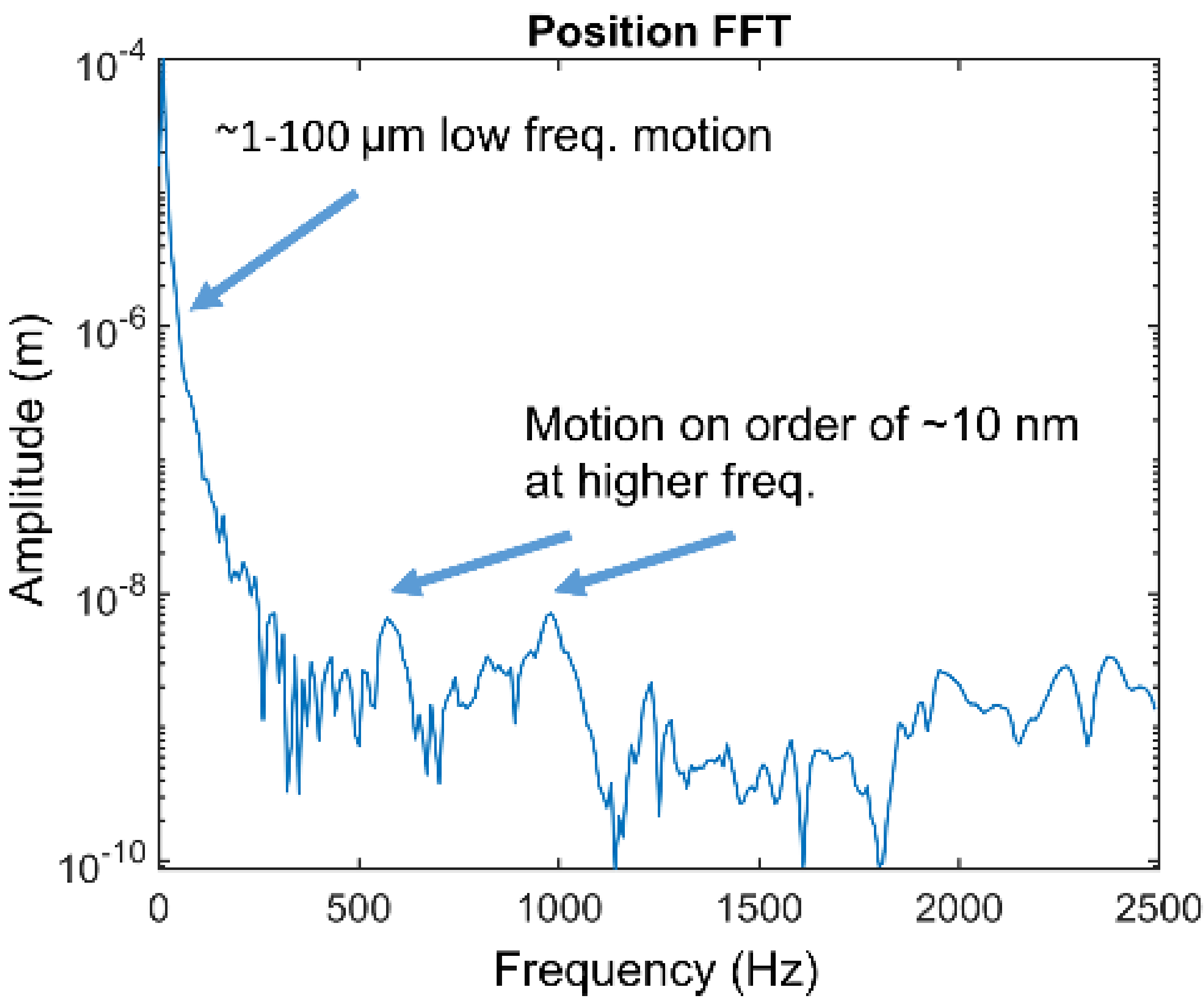
Position FFT
~1-100 µm low freq. motion
Motion on order of ~10 nm
at higher freq.
Amplitude (m)
10-4
10-6
10-8
10-10
0
500
1000
1500
2000
2500
Frequency (Hz)

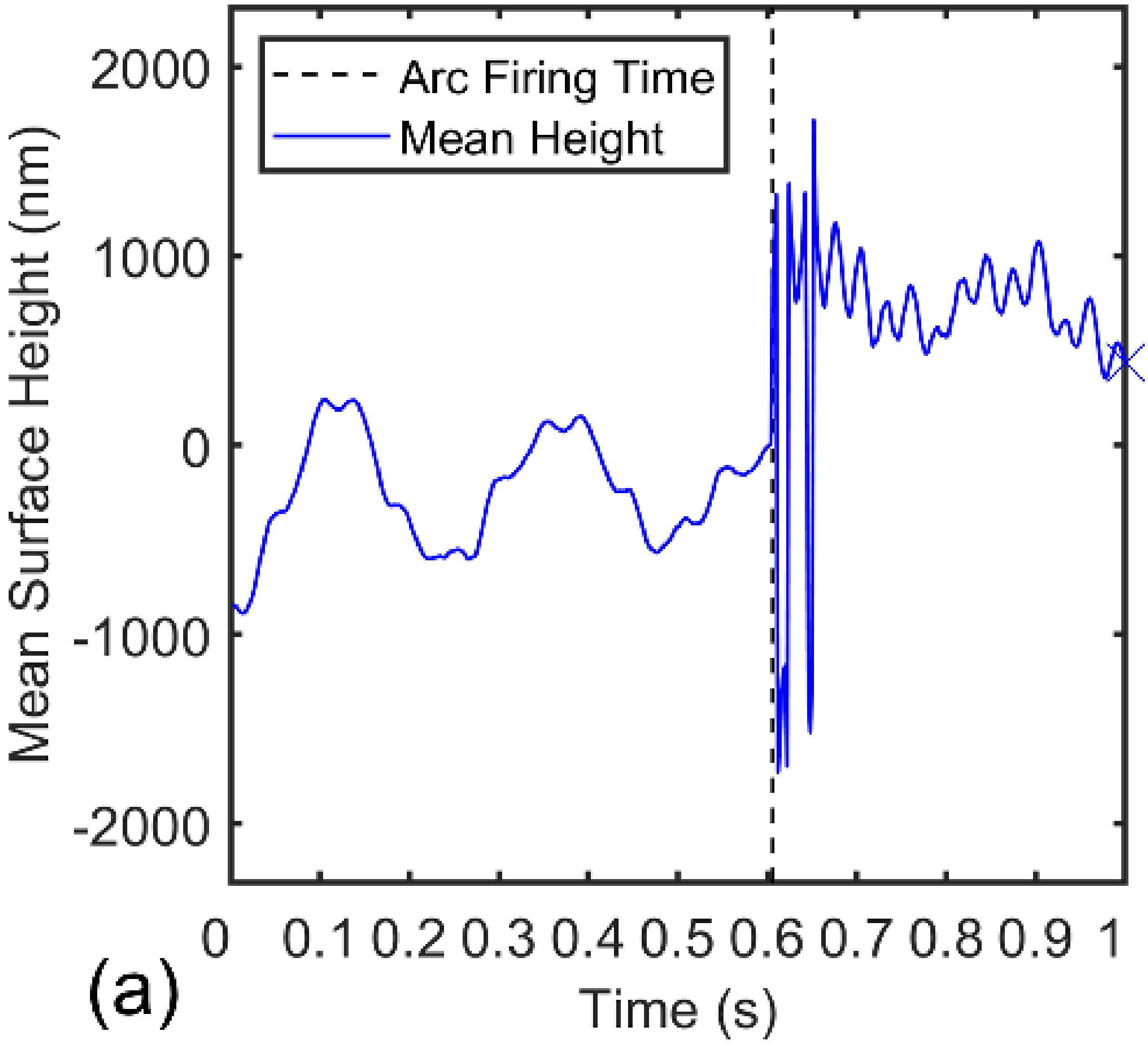
Arc Firing Time
Mean Height
Mean Surface Height (nm)
2000
1000
0
-1000
-2000
0
0.1
0.2
0.3
0.4
0.5
0.6
0.7
0.8
0.9
1
Time (s)

(a)

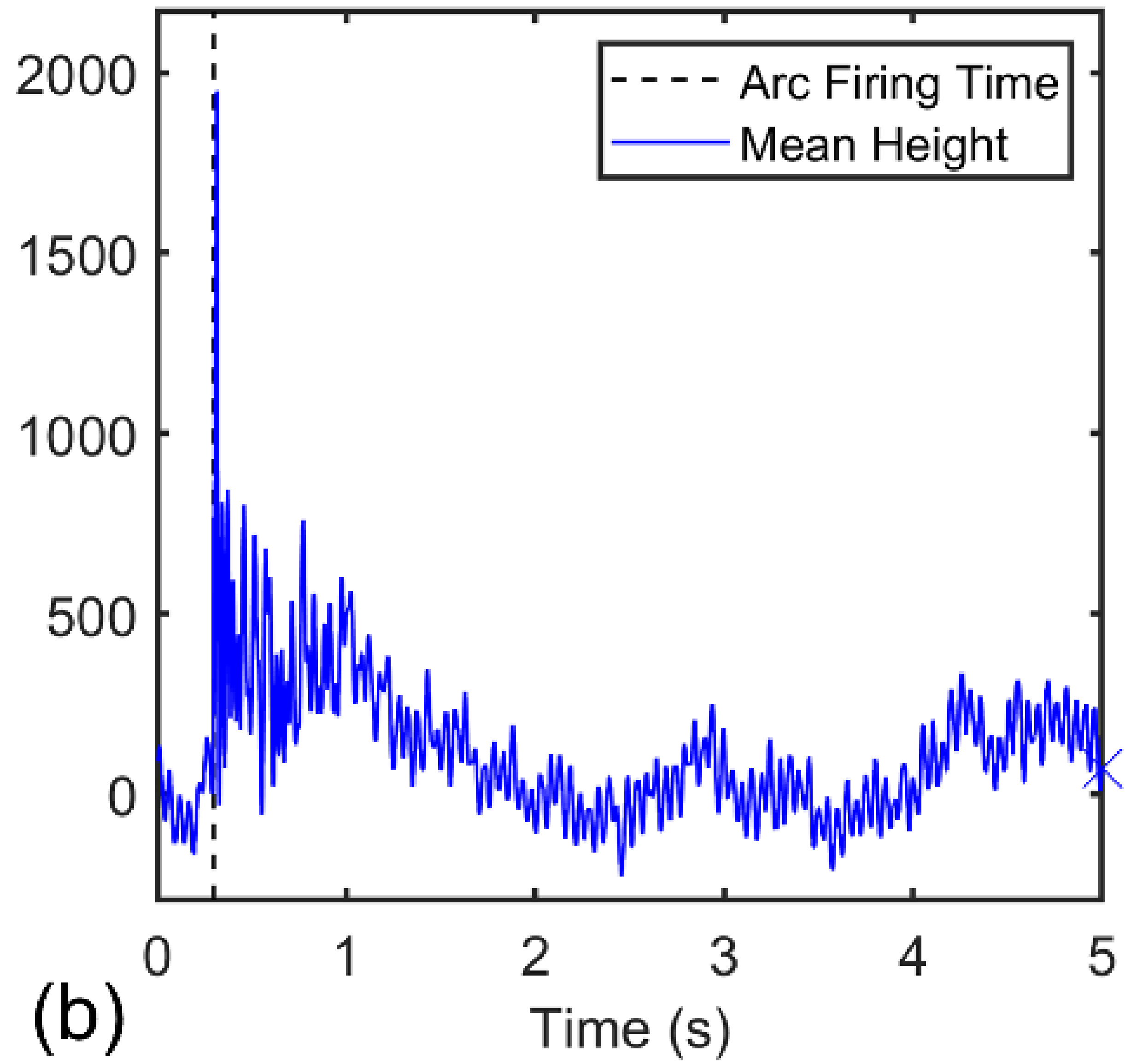
Arc Firing Time
Mean Height
2000
1500
1000
500
0
0
1
2
3
4
5
Time (s)

(b)

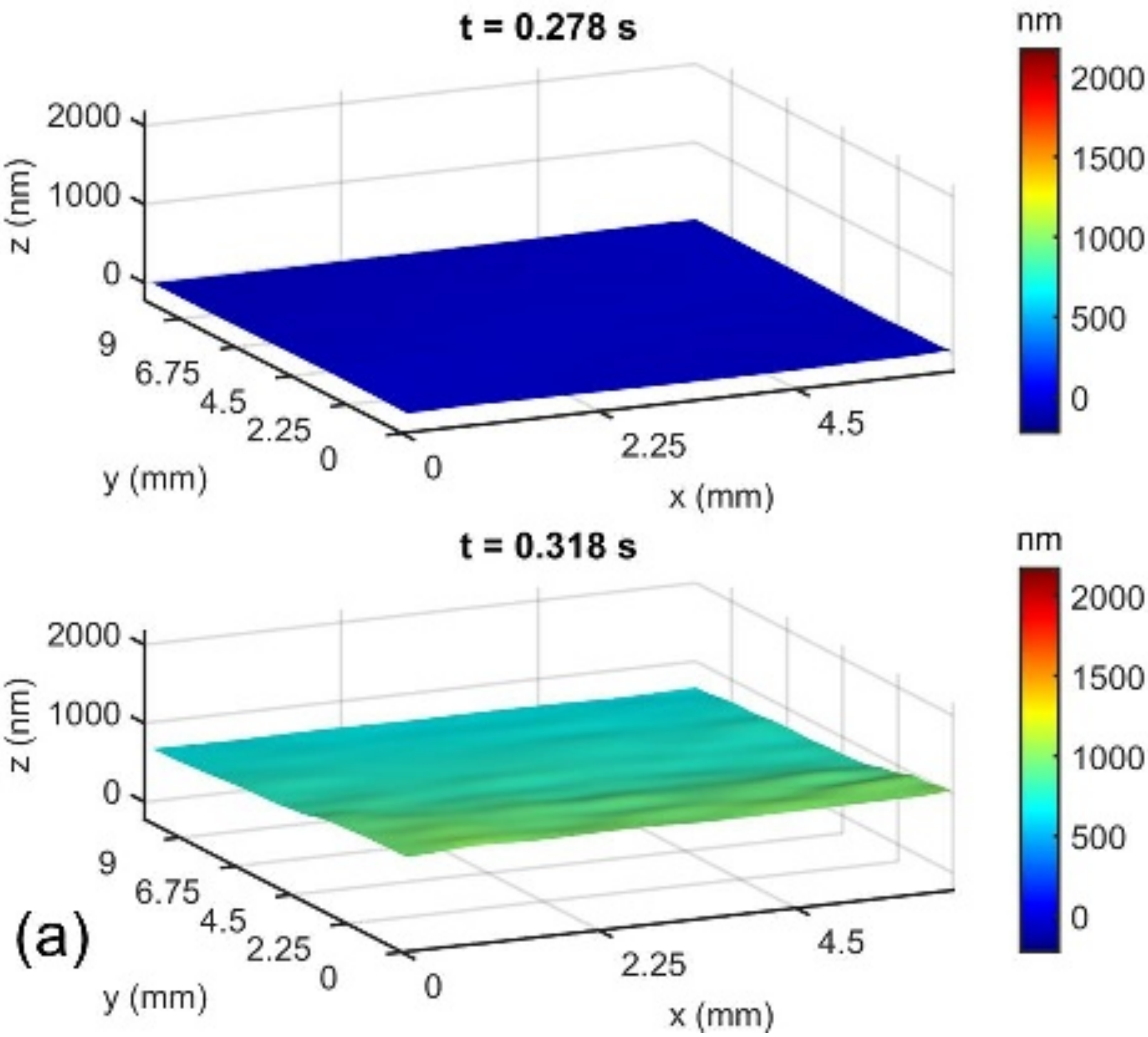
t = 0.278 s
z (nm)
2000
1000
0
y (mm)
9
6.75
4.5
2.25
0
x (mm)
0
2.25
4.5
nm
2000
1500
1000
500
0
t = 0.318 s
z (nm)
2000
1000
0
(a)
y (mm)
9
6.75
4.5
2.25
0
x (mm)
0
2.25
4.5
nm
2000
1500
1000
500
0

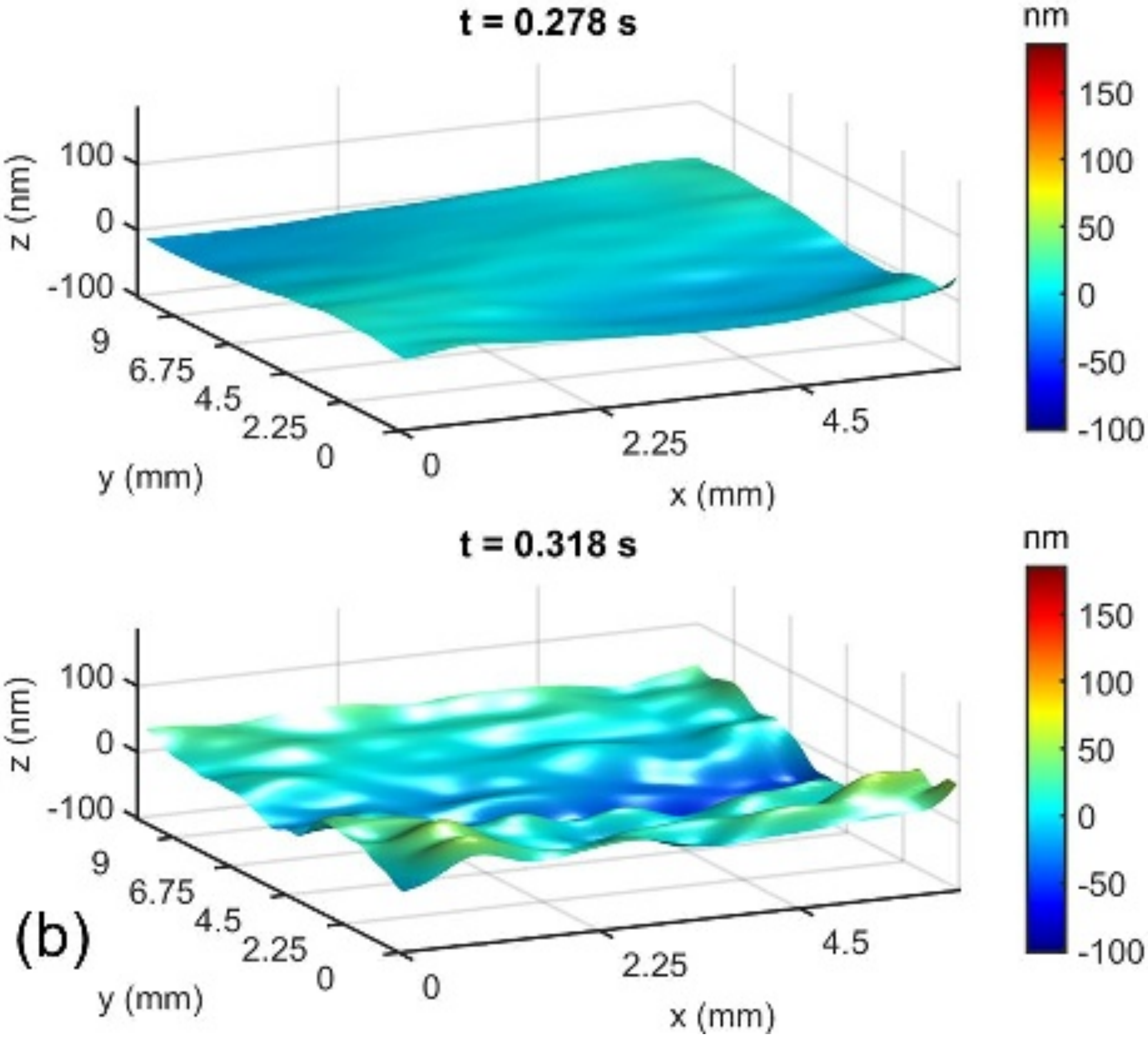
t = 0.278 s
z (nm)
100
0
-100
y (mm)
9
6.75
4.5
2.25
0
x (mm)
0
2.25
4.5
nm
150
100
50
0
-50
-100
t = 0.318 s
z (nm)
100
0
-100
(b)
y (mm)
9
6.75
4.5
2.25
0
x (mm)
0
2.25
4.5
nm
150
100
50
0
-50
-100

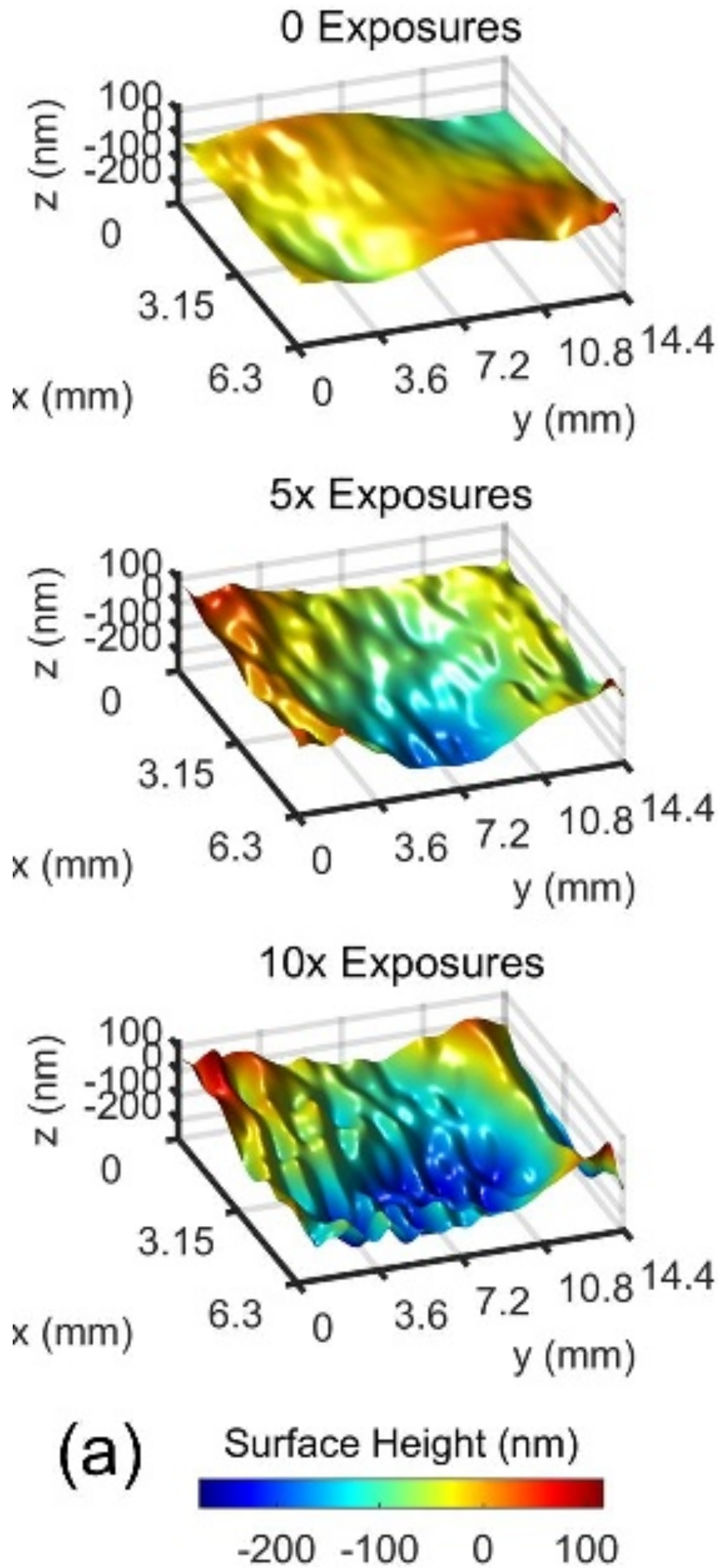
0 Exposures
5x Exposures
10x Exposures
z (nm)
100
0
-100
-200
x (mm)
0
3.15
6.3
y (mm)
0
3.6
7.2
10.8
14.4
(a)
Surface Height (nm)
-200
-100
0
100

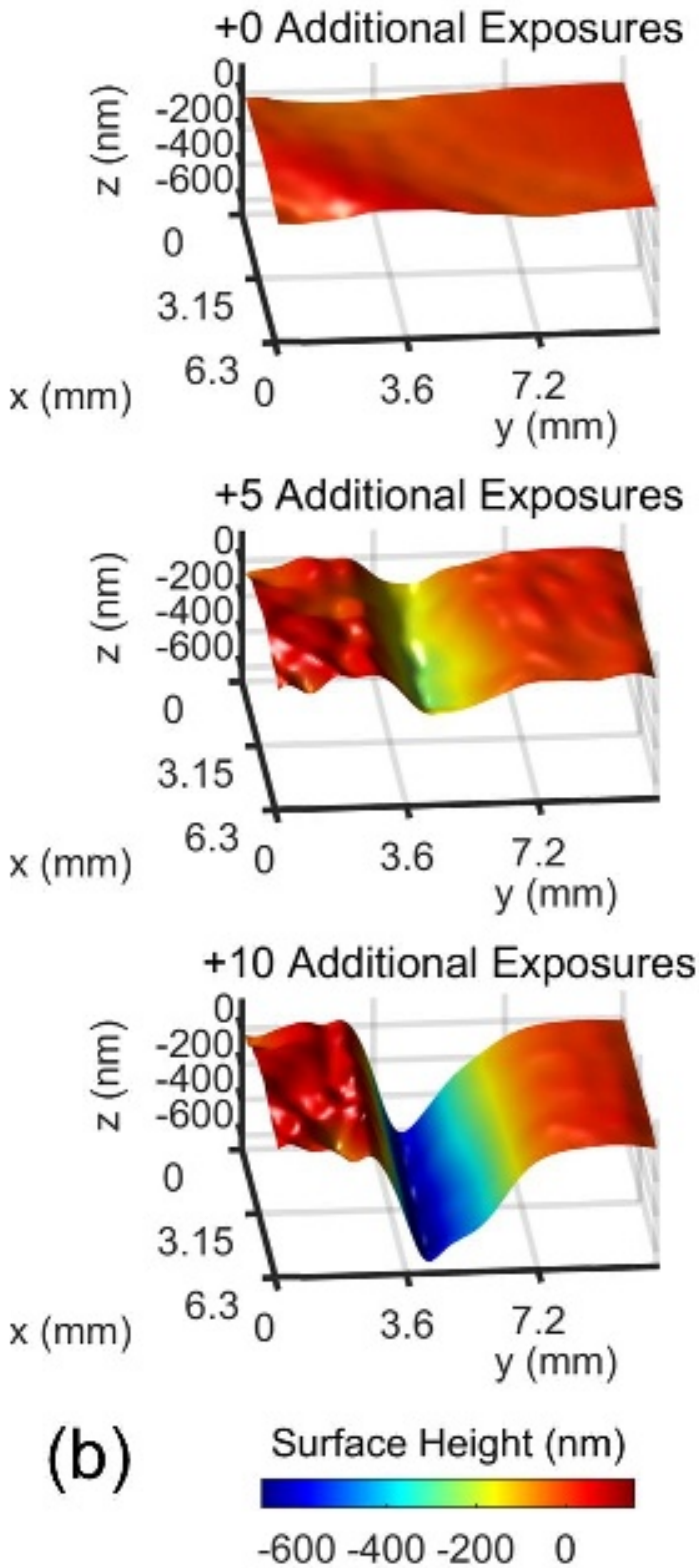
+0 Additional Exposures
+5 Additional Exposures
+10 Additional Exposures
z (nm)
0
-200
-400
-600
x (mm)
0
3.15
6.3
y (mm)
0
3.6
7.2
Surface Height (nm)
-600 -400 -200 0

(b)

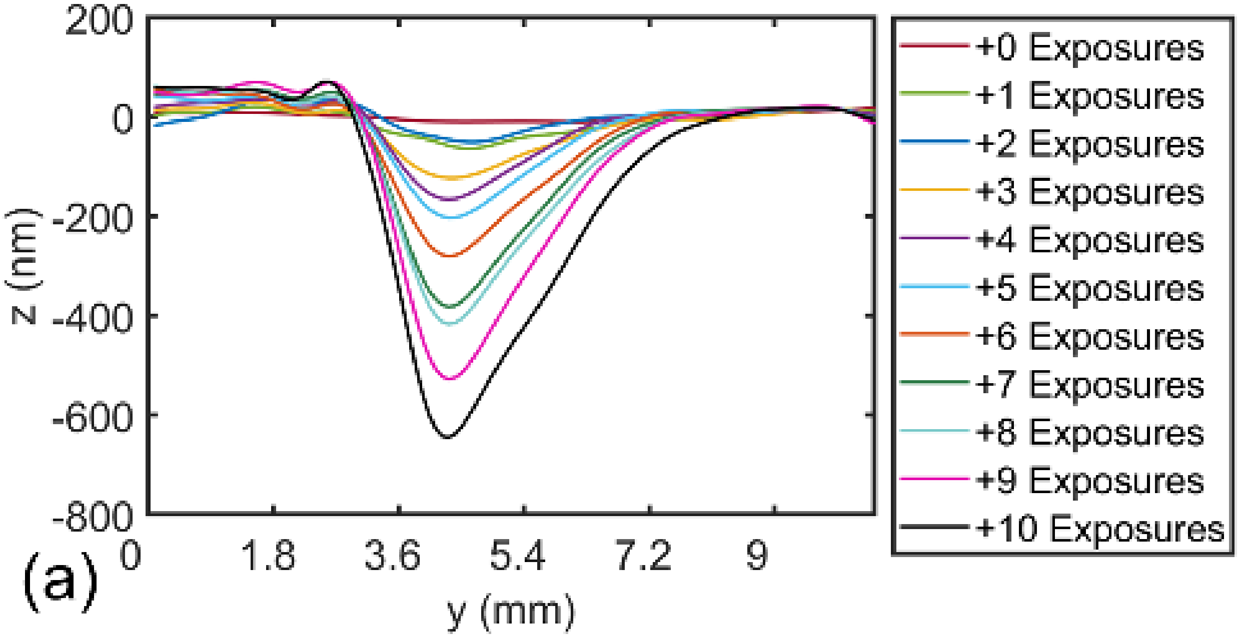
200
0
-200
-400
-600
-800
z (nm)
0
1.8
3.6
5.4
7.2
9
y (mm)
(a)
+0 Exposures
+1 Exposures
+2 Exposures
+3 Exposures
+4 Exposures
+5 Exposures
+6 Exposures
+7 Exposures
+8 Exposures
+9 Exposures
+10 Exposures

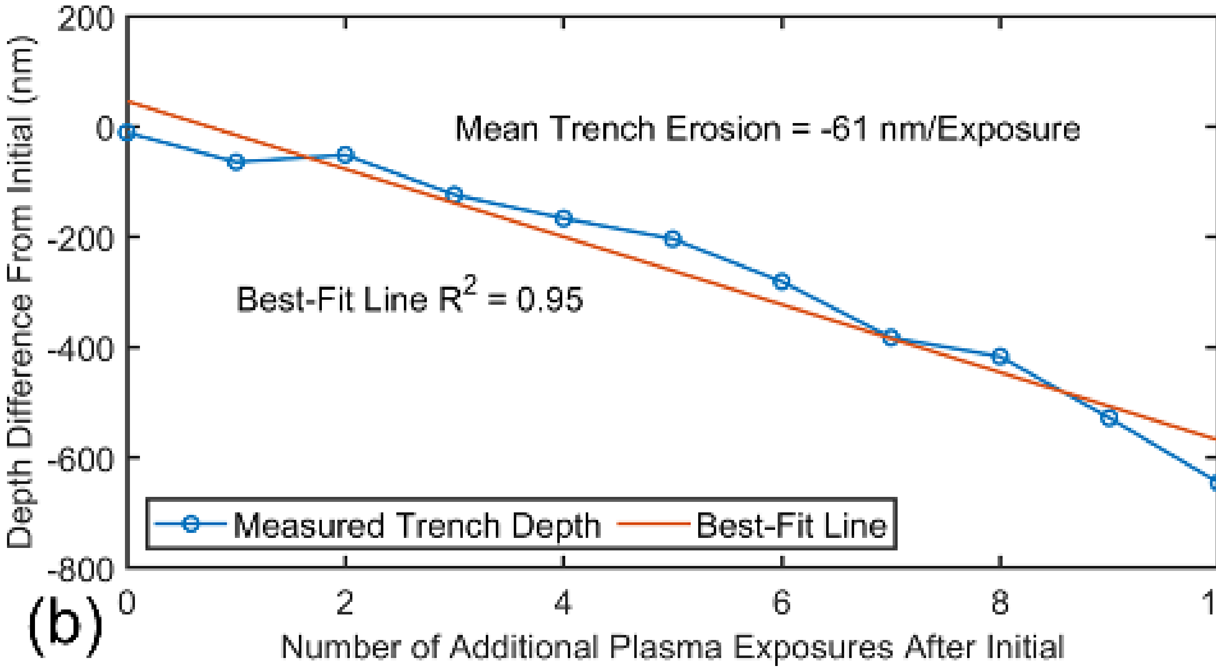
Mean Trench Erosion = -61 nm/Exposure
Best-Fit Line R^2 = 0.95
Measured Trench Depth
Best-Fit Line
Depth Difference From Initial (nm)
Number of Additional Plasma Exposures After Initial
200
0
-200
-400
-600
-800
0
2
4
6
8
10
(b)